Chapter 3

Water column optics and penetration of UVR

Bruce R. Hargreaves

Table of contents

Abstract

Penetration of ultraviolet radiation (UVR) into natural waters depends on the concentration and optical qualities of dissolved organic matter (DOM), phytoplankton, other suspended particles, and on the optical properties of pure water. Optical classification schemes developed for lakes or ocean regions, and relevant to UVR penetration, indicate which of these factors contribute to underwater attenuation of solar radiation. In most cases the best predictor of UV attenuation is optical absorption by chromophoric DOM (CDOM). In natural waters in which UVR penetration is greatest (Crater Lake, USA, and Lake Vanda, Antarctica), CDOM and phytoplankton are so scarce near the surface that UV attenuation by water molecules is significant. Recent evidence from these lakes supports a downward revision of older estimates for UV attenuation by pure water. Variations in atmospheric scattering, sun angle, and depth can cause diffuse attenuation measurements to deviate from the Beer–Lambert Law, but a simple correction is available. Bio-optical models to predict the penetration of UVR into natural waters from measurements will require better understanding of specific absorption of CDOM and phytoplankton, of the reactivity of CDOM, and of the linkage between the microbial community and autochthonous production of CDOM. Spatial and temporal patterns relating UV attenuation with dissolved organic carbon (DOC) concentration and optical quality in aquatic ecosystems appear to be driven by the rates of DOC flux and photobleaching, and by hydrologic properties (residence time and evaporation rate).

3.1 Introduction and background

The penetration of UVR into natural waters leads to exposure of organisms and nonliving matter to energetic photons. The response of organisms and nonliving matter to UVR exposure may change the UV transparency of the aquatic environment. When the intensity (irradiance) of UVR underwater is sufficient to cause biotic damage then a stressful range of depths exists in the water column. Ecological consequences of this stress will depend on the depth of penetration and spectral shifts in the underwater irradiance relative to the depth of the mixed layer ([1], Chapter 4). Spectral shifts may influence vision and behavior of aquatic organisms, especially those with UVR receptors (Chapter 14). They may also influence survival and productivity of aquatic organisms because of the interplay between damaging UV-B wavelengths and the sometimes-beneficial UV-A wavelengths ([2], Chapters 11–13). Ecologists can benefit from improved understanding of patterns and determinants of the intensity and spectral quality of underwater UVR, especially in view of future changes in global climate and in stratospheric ozone. While column ozone and clouds have a strong influence on damaging UVR that reaches the Earth's surface, other factors, especially the concentration and optical qualities of DOM, are more important to the penetration of UVR in the water column.

The topic of underwater optics has been extensively treated with a marine

emphasis by Preisendorfer [3], Jerlov [4], and Mobley [5], and with added coverage of freshwater systems and photosynthesis by Kirk [6]. Reviews of solar radiation penetration into natural waters began with Smith and Tyler [7], and with emphasis on UVR and varying emphasis on marine and freshwater environments include Smith and Baker [8], Baker and Smith [9], Kirk [10], Booth and Morrow [11], and Whitehead et al. [12]. Xenopoulos and Schindler [13] recently reviewed underwater UVR in the context of terrestrial ecosystems and climate change. While marine and freshwater systems are often treated separately in the optical literature, here their optical properties will be compared to reveal common features as well as information gaps and different approaches used by oceanographers and limnologists.

Solar radiation is typically measured underwater as irradiance, the energy striking a unit of surface area (e.g., W m^{-2}), and is further characterized by its wavelength (units, nanometers, nm). Spectral irradiance is reported as energy integrated over a waveband, which may be narrow (e.g., 1 nm) or broad (e.g., UV-A, 320–400 nm; UV-B, 280–320 nm). The solar UVR spectrum, about 10% of the incoming energy reaching the Earth's surface, includes UV-A and UV-B wavebands. Photosynthetic organisms use wavelengths starting at about 400 nm and extending to 700 nm (Photosynthetically Active Radiation or PAR) in the process of photosynthesis. Roughly half of the incoming solar energy is represented by infrared wavelengths from 700 to 2000 nm. Ozone in the atmosphere and DOM in natural waters strongly absorb UV-B wavelengths. Water molecules in the atmosphere and in aquatic systems strongly absorb far-red and infrared wavelengths.

UVR will pass through the air–water interface if it is not reflected. Reflection depends on the angle of incidence and follows Fresnel's Law [6]. Penetration of irradiance coming directly from the sun depends on the solar zenith angle (SZA) for a flat (calm) surface and decreases as SZA rises (i.e. for decreasing sun elevation). Windy conditions can increase the penetration of direct solar irradiance for high SZA but may have the opposite effect at low SZA. Penetration of the diffuse component of sunlight has been modeled [14,15]. The proportions of direct and diffuse solar radiation vary with wavelength, atmospheric conditions, and sun angle (some examples are shown in Figure 4A below). For UV-B wavelengths the distribution is often similar to that for all wavelengths under an overcast sky or when the sun is near the horizon, when models predict 96% transmission, [14]. The effects of surface waves and variations in direct versus diffuse radiation combine to complicate the interpretation of optical field measurements at shallow depths unless temporal and spatial averaging are adopted at appropriate scales [16].

Underwater light is similar in many coastal and freshwater environments. Figure 1 shows an example of underwater UVR and PAR spectra at several depths in a typical coastal ocean site (San Diego, California; unpublished data provided by J.H. Morrow). Water absorbs strongly in the red and longer wavelengths (>600 nm) with the result that the right side of the curves shows rapid attenuation with depth. Photosynthetic pigments in phytoplankton (such as chlorophyll *a*) absorb blue (450 nm) wavelengths most strongly but phyto-

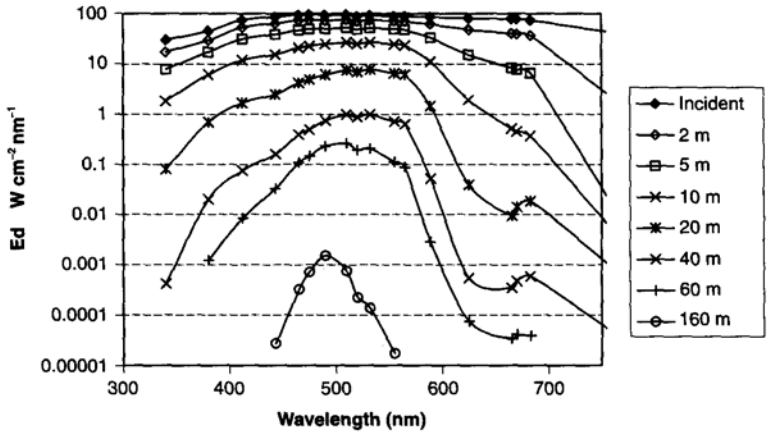

Figure 1. Typical coastal ocean underwater spectra of downwelling cosine irradiance with moderate levels of CDOM and algae. San Diego coastal waters, 5 miles offshore (5 January 2000), using Biospherical Instruments PRR-800 multichannel reflectance profiler (J.H. Morrow, unpublished data). This spectrum is plotted on a log scale to show similar percentage changes over the range of intensity that spans seven decades of magnitude. Except for the peak around 685 nm (caused by algal fluorescence), deep irradiance beyond 520 nm is likely to be caused by Raman scattering from shorter wavelengths.

plankton also absorb at shorter wavelengths. For the component of DOM called CDOM, absorption increases exponentially from the mid-visible wavelengths into the UVR range. The red peak (centered at 685 nm) that is evident at greater depths (most noticeable in the 20 m curve of Figure 1) is fluorescence emitted by photosynthetic cells – a small fraction of the visible light they absorb. The characteristic spectrum of underwater light (note the blue–green peak at 500 nm in the 160 m curve of Figure 1) is caused by combining the strong red absorption of water, the blue absorption by photosynthetic cells, and the violet and UVR absorption by DOM. The color of light emerging from deep natural waters is a product of this selective absorption of the medium and backscattering in the upward direction that increases at shorter wavelengths.

UV transparency of natural waters can be described empirically by two measures that are wavelength-specific and inter-related: the *downwelling diffuse attenuation coefficient*, K_d, and the *percent attenuation depth*, $Z_{n\%}$. A downwelling diffuse attenuation coefficient is nominally proportional to the concentration of substances in the water that absorb or scatter UVR [17,42]. It is typically calculated for specific wavelengths (λ) from measurements of downwelling irradiance ($E_{d,\lambda}$) by fitting the following equation (in units of m^{-1}) [8] to irradiance versus depth data:

$$E_{d(Z,\lambda)} = E_{d(0-,\lambda)}\, e^{(-K_{d,\lambda}*Z)} \quad (1)$$

where Z is geometric depth measured in vertical metres from the mean surface, $E_{d,0-}$ represents downwelling irradiance just below the water surface, and $E_{d(Z,\lambda)}$ is the downwelling irradiance at depth Z (m) and wavelength λ (nm). Figure 2

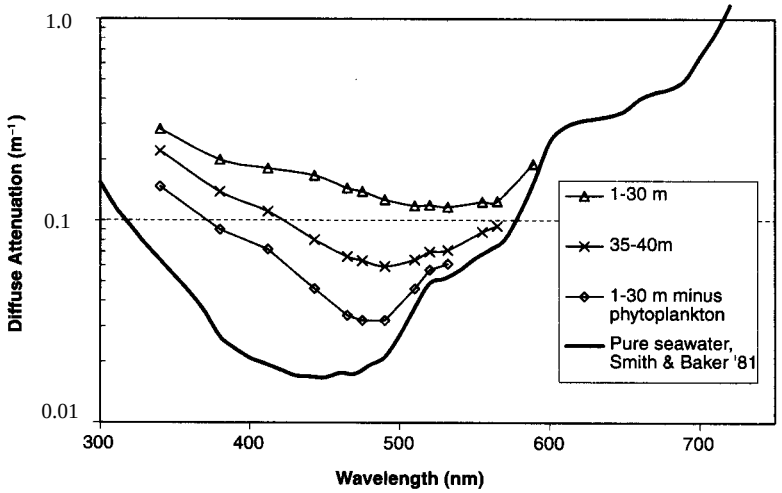

Figure 2. Spectral diffuse attenuation of downwelling irradiance from Figure 1 compared with K_w for pure seawater estimated by Smith and Baker [18]. The phytoplankton concentration (based on chlorophyll *a* fluorescence) was highest in the upper 30 m. The curve labeled "K_d 1–30 m minus phytoplankton" was calculated by regression of spectral K_d against chlorophyll fluorescence for a range of depths, a method that also removes effects of scattering and absorption (including that of CDOM) that covary with phytoplankton fluorescence.

shows diffuse attenuation spectra computed from irradiance data shown in the previous figure. In this example the upper mixed layer of water shows the highest attenuation because of the higher concentration of phytoplankton there. Compared to surface waters, the spectral attenuation at 35–40 m depth is reduced in the blue and UV wavelengths because the chlorophyll concentration is 42% lower than at shallower depths. To show the residual effects on spectral attenuation caused by other substances (DOM and suspended non-algal particles), adjusted K_d values were calculated (by regression of K_d versus algal biomass as estimated from chlorophyll fluorescence) and are plotted as "1–30 m minus phytoplankton" in Figure 2. An estimate of attenuation by pure seawater, K_w, from Smith and Baker [18] is presented as a contrast to "K_d minus phytoplankton" and suggests the magnitude of attenuation by these other substances. Subtracting K_w from "1–30 m minus phytoplankton" yields an exponential curve (exponent = −0.015) typical of CDOM (Figure 6 below).

Rearranging equation (1) and substituting the symbol ζ (Greek "z") for $\mathrm{Ln}(E_{d,0}-/E_{d,z})$, yields Kirk's [6] general equation for the depth (in meters) at which irradiance for a specific wavelength is reduced from 100% just below the surface to n% in a uniformly mixed water column:

$$Z_{n\%,\lambda} = \zeta / K_{d,\lambda} \tag{2}$$

Kirk [6] calls ζ the "optical depth" while Mobley [5] uses "optical depth" differently. Using Kirk's definition for ζ, and using f for the fraction of surface irradiance reaching $Z_{n\%}$, the general solution for optical depth is $\zeta = \mathrm{Ln}(f^{-1})$ with

$\zeta = 1$, 2.3, and 4.6 corresponding to $(f \times 100) = 37\%$, 10%, and 1% respectively. Calculations of $Z_{10\%}$ and $Z_{1\%}$ have been used increasingly in the UV literature [e.g., 10,12,19], but infer significance primarily from the PAR waveband where $Z_{1\%}$ is considered the bottom and $Z_{10\%}$ the midpoint of the euphotic zone for photosynthesis [6]. No general name for these measures is generally accepted, although Williamson [20,21] used Z_a (which he referred to as "the attenuation depth") for the specific case of the 1% attenuation depth. This author suggests that $Z_{n\%,\lambda}$ be referred to as the "% attenuation depth" to serve as a general term for the depth at which irradiance is reduced to $n\%$ of the value just below the surface. Equation (2) can be reduced to:

$$Z_{37\%,\lambda} = 1/K_{d,\lambda} \tag{3}$$

Lacking biological or physical significance for a particular percentage within UV wavelengths, the 37% attenuation depth has the advantage that it is less likely to extend below the mixed layer in the water column. Because K_d is typically determined from mixed layer measurements, the 1% and 10% attenuation depths are more likely to misrepresent the penetration of UVR (specifically, whenever the computed value of $Z_{n\%}$ extends below the mixed layer). This is because K_d often changes below the mixed layer, either increasing (e.g., Figures 5A and 12, also [22–24]) or decreasing (e.g Figure 2, also [19]) compared to surface K_d values. Figure 3 (adapted from Whitehead et al. [12] using data from Table 1) shows $Z_{37\%}$ attenuation depths for 320 nm UVR for the mixed layer at a number of freshwater and marine sites. Also included in Figure 3 are estimates for pure water calculated by Smith and Baker [18] and a new estimate for pure water (described in Section 3.3.4).

The diffuse attenuation coefficient (K_d) is one of several "apparent optical properties" (AOPs) of natural waters described by Preisendorfer [25]. Unlike inherent optical properties (IOPs) described below, AOP's depend on the quality of incident light as well as the optical qualities of the water. In spite of this apparent limitation (and in part because the differences between AOP's and IOP's were said to be small in many instances [26]), a case was argued for the standard use of K_d to characterize natural waters for purposes of optical comparisons and bio-optical models [27,28]. Gordon [17,29] provided a practical means to adjust K_d measurements to remove much of its dependence on the ambient light field. In particular, Gordon [17] established that, after adjustment (described below), $K_{d,0}$ averaged from surface to $Z_{10\%}$ is proportional to the summed concentrations of constituent optical compounds.

In contrast to AOP's, "inherent optical properties" (IOP's) depend solely on the water and its optically active constituents. The IOP's include the beam absorption coefficient "α", beam scattering coefficient "b", and beam attenuation coefficient "c", which are related as follows:

$$c = \alpha + b \tag{4}$$

The absorption coefficient "α" is the sum of absorption by constituent components (including the solvent, water) and is proportional to the concentration of absorbing substances. Similarly, the scattering coefficient is the sum of constitu-

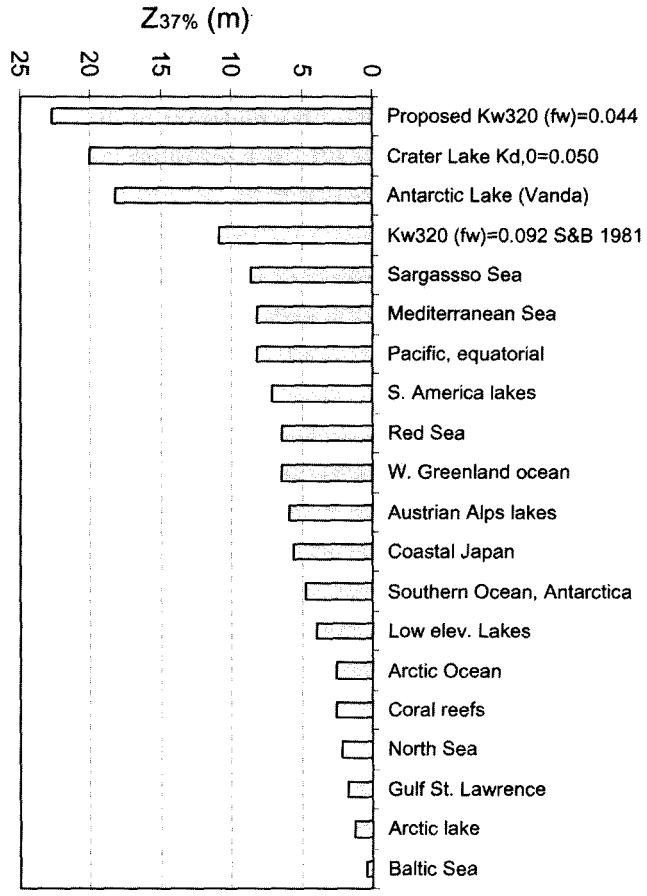

Figure 3. Maximum 37% attenuation depths for 320 nm (depth where irradiance is attenuated to 37% of the value just beneath the surface, computed as $1/K_{d320}$). Values have been calculated for the lowest K_d's reported for each category from Table 1.

ent component scattering and is proportional to the concentration of scattering substances. These three IOPS's are expressed in units of m^{-1}.

A property of the light field that relates AOPs with IOPs is the mean cosine ($\bar{\mu}$). It summarizes the angular distribution of photons according to equation (5). Direct measurement of $\bar{\mu}$ combines downwelling irradiance (E_d, with cosine response to solar zenith angle, maximal to vertical light from above and no response to horizontal light or light from below), upwelling irradiance (E_u), and scalar irradiance (E_o, equal response to light from any direction):

$$\bar{\mu} = (E_d - E_u)/E_o \tag{5}$$

Underwater $\bar{\mu}$ varies with sky and water conditions, the angle of the sun from vertical (solar zenith angle), wavelength, and depth [17]. From equation (5) one can establish a theoretical value (assuming no scattering) of 1.0 for a collimated

beam from above, -1.0 for a beam from below, and zero for a completely diffuse light field. Direct measurements of scalar irradiance have not been reported using commercial underwater UV instruments although Danish scientists have reported upwelling and downwelling scalar irradiance and corresponding values for $\bar{\mu}_d$ and $\bar{\mu}_u$ [117]. Commercial underwater radiometers are available for determining spectral reflectance ratios for visible and UV wavelengths (E_d, E_u, and also upwelling radiance L_u). Stramska et al. [30] have proposed and tested a method to calculate $\bar{\mu}$ as well as α and b_b (the backscattered portion of b) from field measurements of E_d, E_u, and L_u in the wavelengths from 400–560 nm. This approach is promising for determining $\bar{\mu}$ over UV wavelengths but it will require validation beyond the currently specified range of wavelengths.

The mean cosine relates "α" and K_d in natural waters when these optical properties describe a narrow waveband. An exact relationship valid for all depths in the absence of any "internal light source" [17,31] is

$$K_d = (1-R)\alpha/\bar{\mu} + RK_u \tag{6}$$

where R is irradiance reflectance (E_u/E_d) and K_u is the diffuse attenuation coefficient for upwelling irradiance. Internal light sources include Raman scattering and fluorescence emitted from DOM or chlorophyll after absorbing light at shorter wavelengths. When $E_u \ll E_d$, and thus when R becomes very small, equation (6) becomes

$$K_d \approx \alpha/\bar{\mu} \tag{7}$$

where $\bar{\mu}$ is less than 1 and thus K_d is greater than "α" to account for the longer mean path traveled by either diffuse or off-vertical sunlight for each vertical metre in the water column. The exact relationship in this form represents Gershun's Law [32]:

$$K_E = \alpha/\bar{\mu} \tag{8}$$

where K_E is the attenuation coefficient for the net downward irradiance, $E_d - E_u$. From the modeling work of Gordon [17], the mean cosine for downwelling irradiance ($\bar{\mu}_d$) also relates $K_{d,0}$ (measured just below the surface) to IOPs at that depth in a useful empirical equation:

$$K_{d,0} = 1.0395(\alpha + b_b)/\bar{\mu}_{d,0} \tag{9}$$

In equation (9) $\bar{\mu}_{d,0}$ is the fraction of downwelling scalar irradiance contributed by downwelling cosine irradiance ($E_d/E_{o,d}$), measured just below the surface, and b_b is the backscattered fraction of b. This relationship was developed for Case 1 waters (described in Section 2) and should be tested for validity in non-Case 1 waters. Other empirical relationships for predicting K_d from IOPs are described in Kirk [6,10].

Underwater spectral UVR measurements have sometimes been summarized by integration over a broad waveband (e.g., for UV-B and UV-A bands in [33] and [34]). The response of a broadband attenuation measurement, whether calculated from a detailed spectrum or measured with a broadband sensor (e.g., PAR), is subject to errors when used to characterize the optical properties of the

water. These errors occur in attempting to characterize a uniform section of the water column (where IOPs are constant) because the effective K_d and effective "central wavelength"' for the waveband will shift with depth and with the magnitude of attenuation [11,35]. In the UV-B waveband, for example, a simple spectral attenuation model can demonstrate that the wideband K_{dUVB} calculated for a specific depth deviates from the surface K_{dUVB} (full solar spectrum) by 12–19% over a range of K_d ($K_{d320}=0.1$–$22\ m^{-1}$) and depths ($Z_{1\%}$–$Z_{37\%}$). For K_{dUVR} the effect is even greater; using published coastal ocean spectral data Booth and Morrow [11] calculated that K_{dUVR} would change 36% with depth (from 0.32 m^{-1} at the surface to 0.25 m^{-1} at 15 m depth, with an asymptote of 0.21 m^{-1} at much greater depth). Instruments with sensor bandwidth of ≤ 8 nm appear to perform well throughout the UV-A and UV-B ranges [36]. Spectral modeling has confirmed this: errors caused by spectral shift for the 8–10 nm bandwidth sensors of a widely-used UV radiometer (the PUV-500 from Biospherical Instruments, Inc.) are in the range of 1% from the surface down to $Z_{10\%}$ and less than 5% down to the limit of detection [35]. If data reduction from full spectral data is required, a better strategy than broadband integration is to present attenuation or irradiance values for several narrow wavebands within the UV-B and UV-A wavelengths.

3.2 Optical classification of natural waters

Natural waters differ optically from one another in color, transparency, and composition. Oceanographers and limnologists have developed different types of optical classification schemes to account for one or more of these attributes, and these are reviewed by Mobley [5] and Kirk [6]. Jerlov [4] was first to establish the concept of optical classifications for regions of the ocean, and described classes of open-ocean and coastal water based on transparency. Morel and Prieur [37] divided ocean waters according to optically dominant constituents: in Case 1 waters, phytoplankton and their products dominate; in Case 2 waters, the dominant constituents are either mineral particles or dissolved organic matter not associated with phytoplankton. Kirk [38] classified inland waters according to optical constituents (**W**, **G**, **A**, and **T** are used alone or in combinations to indicate the role of **W**ater, **G**ilvin = CDOM, **A**lgae = Phytoplankton, and **T**ripton = inorganic particles). Prieur and Sathyendranath [39] proposed a similar optical classification system for seawater. Kirk's scheme is used below in the description of different optical constituents of natural waters.

The terms DOM, DOC, and CDOM can be confusing and are sometimes used interchangeably. DOM describes the uncharacterized dissolved organic matter in natural waters. While DOM concentration could be quantified on a dry-mass basis (g m^{-3}) and values are found in the older literature, current analytical techniques (e.g., high temperature oxidation [40]), are calibrated in terms of the concentration of carbon atoms. The term DOC is now used when specific concentrations are reported. A molar or mass-based carbon concentration (e.g., g C m^{-3}) is thus the preferred unit of measure for either DOM or DOC. In

contrast to these measures, CDOM is a generic description of the "optical concentration" of DOM, or the concentration of colored substances such as humic and fulvic acids. CDOM is measured as a spectral absorption coefficient ($\alpha_{cdom,\lambda}$) with units of m^{-1}.

Table 1 summarizes data on UV optical properties of natural waters from different regions. Section A describes marine sites while Section B describes freshwater sites. Each section presents UV-A and UV-B values, and entries are nominally sorted by value of attenuation or absorption coefficients. Attenuation, absorption and scattering coefficients have been converted, where feasible, to either 380 or 320 nm for easier comparison. The values of $K_{d,380}$ in the marine environment range from 0.03–0.8 m^{-1}; in freshwater the range is 0.02–32 m^{-1}. The values for $K_{d,320}$ in the marine environment range from 0.07–37 m^{-1}; in freshwater the range is 0.05–165 m^{-1}. The lowest values are found in open ocean (Sargasso Sea and eastern Mediterranean) and deep lakes (Crater Lake and L. Vanda). These low values occur in environments where the "hydraulic residence time" is long and where the water is isolated from terrestrial sources of DOM and nutrients either by distance from land, high elevation, or high latitude. In most cases this UV-transparent water is also exposed to high levels of UVR. The values for K_{dUV} in the region of the Baltic Sea and North Sea [41] and other coastal areas with large rivers [42] tend to vary with salinity in response to mixing of high-CDOM waters discharged by major rivers with low-CDOM waters from the open ocean. UV attenuation has been reported rarely in turbid systems (but see [49]). High values in Table 1 reflect either high DOM loading or evapoconcentration. UVR in lakes and estuaries where erosion or bottom resuspension contribute to extremely high turbidity can be assumed to exhibit rapid attenuation with depth.

3.3 Constituents controlling UV attenuation in natural waters: bio-optical models

Bio-optical models have been developed to predict spectral attenuation as a function of conveniently measured parameters and are discussed extensively in Mobley [5] and Kirk [6]. Since the pioneering work of Smith and Baker [42], bio-optical models typically break down diffuse attenuation into optical constituents of natural waters. In an approach covering UV-B and UV-A wavelengths summarized by Baker and Smith [9,43], these components are represented as partial attenuation coefficients (λ for each term not shown for simplicity):

$$K_{d\ Total} = K_{d\ Water} + K_{d\ CDOM} + K_{d\ Phyto} \tag{10}$$

to which $K_{d\ Tripton}$ may be added for waters where attenuation is caused by nonliving particles.

These components can be individually computed from measurements at a site after proper "calibration" to establish "specific attenuation" factors. For example, from a series of sites that differ in DOC concentration and having low or constant levels of phytoplankton pigments, $K_{d\ total}$ and [DOC] are measured

Table 1. UV optical properties, ranked in order of UV transparency

Site	WL (nm)	$c=\alpha+b$	b_w	α_w (m^{-1})	α_{cdom} (m^{-1})	α_p (m^{-1})	K_d (m^{-1})	Source
A. Ocean and coastal measurements								
UV-A ocean data								
Pure seawater (see Freshwater table for α_w)								
Pure seawater	380		0.0094					Morel 1974 in [6]
Clearest natural waters	380	[0.031]		0.022			0.027	Smith & Baker [18]
Sargasso Sea	380						0.044–0.045	Tyler & Smith [110]
East Mediterranean	375						0.05	Jerlov [95]
Gulf of Mexico USA	380						0.06	Smith & Baker [8]
Eastern Pacific (Mexico)	380						0.075	Tyler & Smith [110]
West Mediterranean	375						0.02–0.08	Højerslev [65]
Antarctica (61°S)	380						0.08–0.15	Helbling et al. [44]
Coastal Japan (3/98–3/99)	380				0.15[a]	0.16[a]	0.09–0.59, 0.24[a]	Kuwahara et al. [108]
Gulf of California (Mexico)	380						0.11–0.28	Tyler & Smith, [110]
Arctic polynya	380						0.18–0.50	Belzile et al. [48]
Tropical, near coral reefs	380						0.18–0.76	Dunne & Brown [111]
Gulf of St. Lawrence	380						0.1–0.8	Kuhn et al. [57]
Gulf coast, Florida USA	380						0.28	Smith & Baker [8]
Continental Slope	365	0.10			0.02			Clark & James '39 in [4]
Bermuda	380	0.20			0.03			Ivanov et al. '61 in [4]
North Sea	375				0.09–0.15			Højerslev [65]
	375				0.16–0.53			Stedmon et al. [77]
Kattegat	380	0.54			0.11	0.3		Jerlov '55a in [4]
	375				0.30–0.68			Højerslev [65]
	375				0.46–0.92			Stedmon et al. [77]
South Baltic Sea	375				0.71–0.90			Stedmon et al. [77]
Baltic Sea	375				0.89–1.04			Højerslev [65]
Delaware Bay mouth USA	380				0.6–1.2			Vodacek et al. [23]
Skagerrak	380				0.1	0.3		Malmberg '64 in [4]
	375				0.12–0.31			Højerslev [65]
	375				0.09–0.42			Stedmon et al. [77]

UV-B ocean data							
Pure seawater	320		0.0200				Morel 1974, in [6]
Pure seawater	320	[0.104]		0.084		0.094	Smith & Baker [18]
Sargasso Sea	320					0.069	Højerslev 1985 in Aas et al. [117]
	310					0.15	Højerslev [65]
East Mediterranean	310					0.15	Jerlov [95]
Central Equatorial Pacific	310					0.15	Smith & Baker [8]
West Mediterranean	310					0.16–0.43	Smith & Baker [8]
Gulf of Mexico, USA	310					0.18	Smith & Baker [8]
Red Sea (Gulf of Aqaba)	310					0.19	Iluz '93 in [10]
Western Greenland	310					0.19–0.21	Højerslev [65]
Orkney – Shetland	310					0.39	Højerslev [65]
Antarctica (61°S)	320					0.21–0.23	Helbling et al. [44]
Arctic polynya	320					0.39–0.83	Belzile et al. [48]
Coastal Japan (3/98–3/99)	320				0.44[a]	0.30[a]	0.18–0.98, 0.52[a] Kuwahara et al. [108]
Tropical, near coral reefs	320						0.39–1.5 Dunne & Brown [111]
Gulf of St. Lawrence	310						0.68–2.0 Kuhn et al. [57]
Gulf coast, Florida USA	310						0.8 Smith & Baker [8]
German Bight, North Sea	310				0.07–1.49		0.53–5.0 Højerslev [65]
Skagerrak	310						0.59–1.20 Højerslev [65]
Kattegat	310						1.2–2.4 Højerslev [65]
Baltic	310						3.0–3.5 Højerslev [65]
Delaware Bay mouth USA	320				1.3–2.8		Vodacek et al. [23]
Yellow Sea	310						32–37 Højerslev '88 in [10]
B. Lake measurements							
UV-A lake data							
(Pure water)	375	0.045		[0.038]			Clark & James '39 in [4]
(Pure water)	380		0.0072				Morel '74 in [3], see also [58]
(Pure water)	380	[0.017]		0.010			Sogandares & Fry [112]
(Pure water)	380	[0.017]		0.010			Pope & Fry [101]
(Pure water)	380					0.018	Hargreaves (unpub. Crater Lake 8/01)
(Pure water)	380	[0.029]		0.022		0.025	Smith & Baker [18]
Crater Lake, Oregon USA	380				0.004–0.009	0.022	Hargreaves (unpub. Crater Lake, 0–20 m 8/01, divided by D_0)

Table 1. (*cont.*)

Site	WL (nm)	$c=\alpha+b$	b_w	α_w (m^{-1})	α_{cdom} (m^{-1})	α_p (m^{-1})	K_d (m^{-1})	Source
B. Lake measurements (*cont.*)								
Crater Lake, Oregon USA	380						0.016–0.33	Hargreaves, Larsen, Girdner (unpub.) Crater Lake, 0–15 m, Jun-Jul '96–'99
Crater Lake, Oregon USA	380						0.022	Tyler & Smith [110]
Lake Vanda, Antarctica	380						0.023	Vincent et al. [68]
12 Lakes, S. Argentina	380				0.05–1.9		0.07–3.0	Morris et al. [60]
Lake Tahoe, USA	380						0.08	Smith et al. [99]
High lake, Austria	380						0.08–0.14	Sommaruga & Psenner [63]
14 Lakes, NE USA	380				0.23–44		0.16–32	Morris et al. [60]
L. Giles, PA USA	380				0.07		0.16	Morris et al. [60]
4 Arctic lakes, Canada	380						0.41–2.8	Laurion et al. [61]
L. Biwa, Japan	380						0.5–7.5	Belzile et al. [49]
18 Subarctic lakes, Canada	380						0.67–16	Laurion et al. [61]
7 Lakes, Canada	380						0.48–9.1	Scully & Lean [33]
20 Lakes, Colorado USA	380				0.51–4.7		1.3–17	Morris et al. [60]
San Vincente Reservoir, San Diego, CA USA	380						2.69	Tyler & Smith [110]
L. Lacawac, PA USA	380				1.45		3.22	Morris et al. [60]
13 Lakes, Alaska USA	380				0.90–7.0		3.7–13	Morris et al. [60]
UV-B lake data								
(Pure water)	313	0.041		[0.027]				Boivin et al. [118]
(Pure water)	320		0.0153					Morel 1974 in [6], see also [58]
(Pure water)	320	0.022		[0.007]				Quickenden & Irvin [113][b]
(Pure water)	320						0.04	Hargreaves, unpub. (Crater L. 8/01)
(Pure water)	320	[0.099]		0.084			0.092	Smith & Baker [18]
Crater Lake, OR, USA	320					0.006-0.017	0.050	Hargreaves, unpub. (0–20 m, 8/01, divided by $D_0=1.13$)

Lake Vanda, Antarctica	320			0.055	Vincent et al. [68]
Crater Lake, OR USA	320			0.051–0.71	Hargreaves et al. (unpub.) 0–15 m, Jun–Jul '96–99
12 Lakes, S. Argentina	320	0.14–6.5[a]		0.14–7.7[a]	Morris et al. [60]
High elev. lake, Norway	320			0.17	Hessen [114]
High elev. lake, Austria	320			0.17–0.26	Sommaruga & Psenner [63], seasonal
11 Lakes (rocky) Alps & Pyr	320	0.21–1.8[a]		0.17–2.5[a]	Laurion et al. [62]
Lake Giles, PA USA	320			0.25–1.6	Hargreaves & Moeller, unpub.[c]
	320	0.23		0.32	Morris et al. [60]
	320		0.1–0.7	0.55–1.3	Ayoub et al. [46]
14 Lakes, NE USA	320	0.23–165[a]		0.32–67[a]	Morris et al. [60]
10 Lakes (trees) Alps & Pyr	320	0.48–4.6		0.60–5.7	Laurion et al. [62]
4 Arctic lakes, Canada				0.75–7.9	Laurion et al. [61]
5 meadow lakes, Alps & Pyr	320	0.74–3.1		0.87–4.3	Laurion et al. [62]
L. Biwa, Japan	320	0.85–6.9		1.1–14	Belzile et al. [49]
7 Lakes, Canada	320			1.1–21.6	Scully & Lean [33]
18 Subarctic lakes, Canada				1.7–41	Laurion et al. [61]
20 Lakes, Colorado USA	320	2.0–17		2.8–37	Morris et al. [60]
13 Lakes, Alaska USA	320	5.8–27		7.1–48	Morris et al. [60]
Lake Lacawac, PA USA	320			6.0–19	Hargreaves & Moeller, unpub.[c]
	320	5.8		7.8	Morris et al. [60]
	320		1.2–10	10–16	Ayoub et al. [46]

[a] Error in either α_{CDOM}, α_p, or K_d likely because $\alpha_{CDOM} + \alpha_p + \alpha_w$ exceeds K_d.

[b] After conversion of decadic beam attenuation value into $\log_e$ (value × 2.303), the spectral attenuation (280–320 nm) was exponentially regressed against wavelength to estimate c_{w320}, then α_{w320} was computed by subtracting scattering coefficient for pure water (b_w).

[c] Seasonal range of K_{d320}, 1993–2001.

(the latter from water samples). Then a regression of $K_{d\ total}$ versus [DOC] is computed to yield the DOC-specific diffuse attenuation factor (K^*_{DOC}) from the regression slope. This approach can also be used to estimate other specific attenuation factors (K^*_{Chl}, $K^*_{Tripton}$) and a similar approach could estimate specific absorption factors as well. In early attempts to estimate K^*_{CDOM} and K_w, Smith and Baker [18] subtracted modeled phytoplankton attenuation spectra from $K_{d,total}$ calculated from natural waters low in CDOM to estimate K_w. Baker and Smith [43] subtracted modeled phytoplankton attenuation spectra (developed as described above) and K_w from $K_{d,Total}$ for coastal waters to estimate $K_{d,CDOM}$. Various non-linear models have been developed to relate absorption and attenuation of algal cultures and natural phytoplankton to chlorophyll *a* concentration [5]. There is some information on UV attenuation by algae [44–51] but numerous studies have focused only on visible wavelengths [30,38,52–56].

The use of partial attenuation coefficients in bio-optical models has been criticized because the measured value of K_d does not depend solely on the natural waters [31]. AOP's such as K_d vary with sun angle, sky conditions, and depth, although some [26] have argued that the effects are small if the sun elevation is reasonably high and thus K_d can be used as a quasi-inherent property. Gordon [17] has established through optical modeling that K_d can be converted into a quasi-inherent optical property, for near-surface conditions at least, if it is first adjusted to remove atmospheric effects using equation (11). The procedure is to measure K_d near the surface or average K_d over 0–10% attenuation depth, and then multiply K_d by $\bar{\mu}_{d,0}$. The adjusted K_d can be expected to respond proportionally to changes in concentration of absorbing substances. Gordon's method for determining $1/\bar{\mu}_{d,0}$ (for which he used the symbol D_0) applies to calm (flat) surfaces of case 1 waters [17]:

$$1/\bar{\mu}_{d,0} = D_0 = f_{direct}/\cos(\theta_w) + 1.197 f_{diffuse} \tag{11}$$

where f_{direct} and $f_{diffuse}$ are the fractions of incident irradiance in the direct rays from the sun and in the indirect skylight respectively. The value of $\cos(\theta_w)$, the angle from the zenith of direct sunlight just beneath the surface after direct sunlight has been refracted from its incident angle ($\cos(\theta_\alpha)$) by passing through the horizontal water surface, can be determined from Snell's Law [6]. For light passing from air to water, $\cos(\theta_w) = \cos(\theta_a)/(n_a/n_w)$, where n_a/n_w is the ratio of refractive indices for air and water (nominally 1.33 in the visible wavelengths but is within 0.3% of 1.345 over the wavelengths 300 nm to 400 nm). Gordon's equation is almost identical to a "mean pathlength" equation derived independently by Zepp and Cline [15] to determine the amount of light absorbed in a vertical metre of water column based on laboratory measurements of absorption coefficients and modeled or measured incident sunlight. Gordon [17] suggests simple adjustments of D_0 for windy conditions that cause surface waves. He recommends using either $K_{d,0}/D_0$ or $K_{d,0-10\%}/D_0$ whenever the objective is to compare inherent optical properties of natural waters. This approach has been mentioned rarely in UVR studies (but see [57]). It will be used later in this chapter to estimate spectral attenuation by pure water.

The values for f_{direct} and $f_{diffuse}$ vary with atmospheric conditions (e.g., aerosols), sun angle, and wavelength. They can be determined with simple field measurements [17]: a vertically oriented radiometer with cosine sensor records full sun and sky, then is partially shaded to block only the direct irradiance from the sun. The ratio $E_{d,shaded}/E_{d,full}$ is $f_{diffuse}$, while f_{direct} is $(1-f_{diffuse})$. Figure 4A shows summer values for $f_{diffuse}$ for extremely clear air at Crater Lake, Oregon (1882 m elevation) and the hazier air over Lake Lacawac, Pennsylvania (400 m elev.) on clear "blue sky" summer days. Under overcast conditions and low solar elevation the value of $f_{diffuse}$ approaches 100% and D_0 (Figure 4B) approaches 1.2. At high solar elevation the longer UV wavelengths become more direct, more so

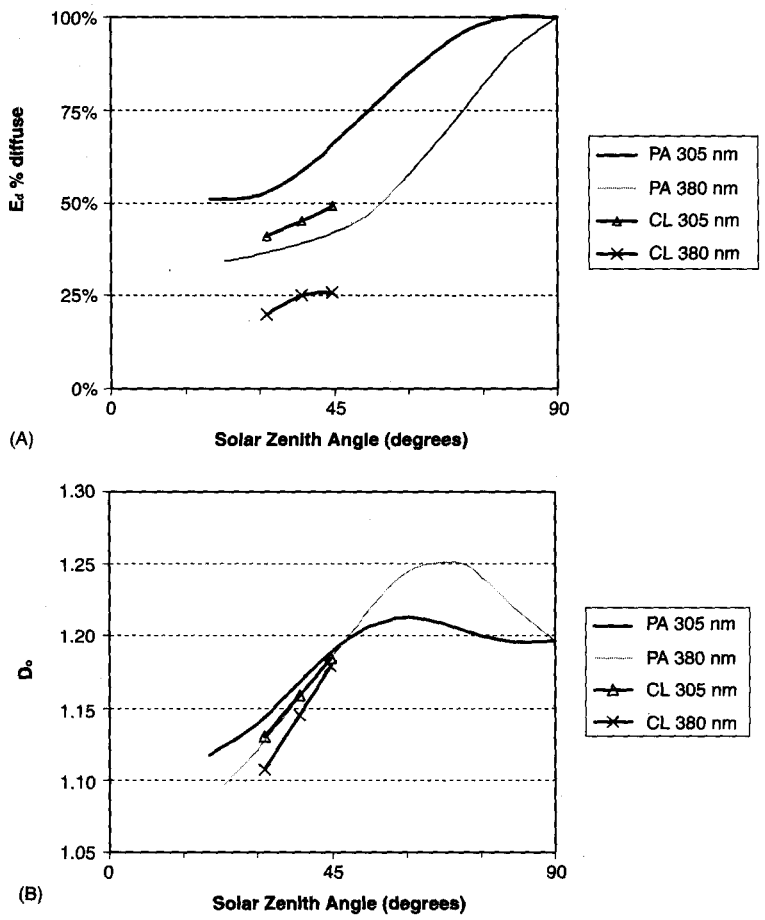

Figure 4. Examples of direct and diffuse solar irradiance and a correction factor for diffuse path length in K_d measurements (Hargreaves, unpublished). (A) Diffuse fraction of irradiance as a function of solar zenith angle during summer, 1996, L. Lacawac, Pennsylvania (41.3°N) and August 2001, Crater Lake, Oregon (42.9°N). (B) Calculated correction [17] to remove effects of irradiance field from near-surface diffuse attenuation (K_d) measurements, based on data in part (A).

in the clean dry air over Crater Lake than over L. Lacawac in the N.E. USA. For this range of conditions D_0 varies from 1.09 to 1.26. The value of $f_{diffuse}$ at 320 nm during summer in the Gulf of St. Lawrence (latitude 47–50°N, solar zenith angle 24–54°) ranged from 48–72% [57]. If K_d measurements are made with SZA $\leq 50°$, the effect of incident diffuse and direct light on K_d will always be less than 20%. At the Latitude (41.3°N) of L. Lacawac, the SZA will be less than 50° if measurements are made within 3 hours of solar noon between the dates of 17 April and 26 August. Before 26 February and after 14 October the SZA will be greater than 50° even at solar noon.

The first spectral models, developed for marine systems by Prieur and Sathyendranath [39] and Baker and Smith [43], emphasized phytoplankton optics, although they included components for attenuation by CDOM, phytoplankton, and water. From these and subsequent studies (reviewed by Morel [58]) has emerged the importance of variation in phytoplankton attenuation per unit of chlorophyll, hereafter referred to as "specific phytoplankton attenuation". While the Baker and Smith [43] model was optimized for UV-B wavelengths and included a CDOM component, this was based on scant data relating optical absorption to the concentration of DOM. When CDOM was detected in the open ocean it was assumed to covary with phytoplankton and often modeled without direct measurement. A recent summary of ocean bio-optical models in Morel [58] does not specifically address UV wavelengths. Yentsch and Phinney [59] mention that the blue and UV regions of algal spectral absorption are the most variable, especially when algae produce UV-absorbing mycosporine-like amino acids (MAA's).

Freshwater optical models relevant to UV attenuation have been developed [33,60,61]. These generally find CDOM is the most important factor, although absorption by phytoplankton and detrital particles [46,49,62,63] or scattering by suspended solids [49] has also been important in some cases. From recent UV investigations in freshwaters has emerged the importance and variability of the CDOM absorption coefficient scaled per unit of DOC concentration, hereafter referred to the DOC-specific absorption factor ($\alpha^*_{\lambda DOC}$). As is the case for marine systems, there are relatively few measurements of UV attenuation or absorption by freshwater phytoplankton [46,49].

Despite an emerging consensus on chlorophyll-specific absorption for visible wavelengths [58], current models appear inadequate to describe the highly variable UV attenuation exhibited by phytoplankton. With regard to DOC and CDOM, several studies (described later) have revealed regional patterns relating K_d and CDOM to [DOC] in relation to climate, precipitation, river discharge, and watershed properties. Integration of patterns and processes to explain UVR penetration into aquatic systems has been lacking.

3.3.1 Role of CDOM (Kirk type G waters)

CDOM was central to the earliest optical models for seawater (Jerlov, 1968 [4]). Interest in CDOM in freshwater goes back to the early 1900's (Shapiro, 1957

[64] cites a 1908 paper on humic substances precipitated from Finnish lakes). It has long been recognized that the penetration of ultraviolet radiation (UVR) depends on concentrations and optical qualities of dissolved organic matter (DOM) [4,65–67]. In non-turbid waters where UV attenuation is high, absorption by CDOM easily surpasses attenuation by other components. Somewhat surprising is the recent finding that CDOM tends to be the most predictive optical component of UV attenuation even in low DOC systems. UV bio-optical models developed recently for lakes reflect a dominating effect of DOC and CDOM, with only a small or immeasurable contribution by phytoplankton in surface waters [33,60,62,68].

Lakes matching Kirk's "Type G" typically have moderate to high levels of DOC. Figure 5 shows an example the close relationship between α_{cdom380} measured in a spectrophotometer and $K_{\text{d,380}}$ calculated from field measurements of underwater irradiance at 380 nm in a moderately clear lake (L. Giles, PA, listed in Table 1). The two signals change together and increase below the mixed layer (9.5 m on this date in early September). Attenuation and α_{cdom} decrease substantially in the mixed layer of this lake during summer months when rates of UVR photobleaching of CDOM exceed the rates of CDOM production and import [22].

In the older literature CDOM has been called "yellow substance", "gelbstoff", and "gilvin'. It is considered to be a mixture of compounds chemically characterized as humic and fulvic acids [6,10,69,70]. Figure 6 shows typical absorption spectra for the CDOM in water from two mid-latitude lakes that has passed through a fine glass fiber filter. The samples are from the depth of the mixed layer of two lakes surrounded by mixed conifer–deciduous forest: L. Giles (watershed soils well-drained) and L. Lacawac (bordered 50% by a sphagnum bog). The values come from absorbance ($A_{\text{sample},\lambda}$) recorded in a spectrophotometer using a quartz cuvette, corrected by subtracting (optically or numerically) the value for highly purified water, $A_{\text{water},\lambda}$, and the cuvette to compute $A_{\text{cdom},\lambda}$. We assume negligible absorbance by inorganic dissolved matter such as ferrous iron, nitrite, or sulfate ions. An adjustment is often made to correct for instrument baseline drift and optical scattering within the cuvette that would otherwise cause errors in estimating $A_{\text{cdom},\lambda}$. A long reference wavelength (λ_{base}) should be chosen for the correction of offset (e.g., >650 nm) where absorption by CDOM is assumed nil; 700 nm or 775 nm are particularly useful in avoiding the strong temperature effects on the absorption of pure water that reach a peak at about 750 nm [71,72] but a longer wavelength (up to 900 nm) may be needed for highly concentrated CDOM. Suggestions for subtracting a spectral scattering term [67,73] from measured A_λ are derived from empirical models showing scattering from small particles in nominally-filtered natural waters varies in proportion to λ^{-1}. Depending on the sample filtration and optical configuration of the instrument and cuvette, spectral scattering may affect the measurement; the suggested correction, $A_{\text{cdom},\lambda} = A_{\lambda\text{cdom\_raw}} - A_{\text{base}}(\lambda_{\text{base}}/\lambda)$, has not been rigorously tested. $A_{\text{cdom},\lambda}$ is then converted into a (Napierian) absorption coefficient, $\alpha_{\text{cdom},\lambda}$ (units m^{-1}):

$$\alpha_{\text{cdom},\lambda} = \text{Ln}(10) A_{\text{cdom},\lambda}/\ell \tag{12}$$

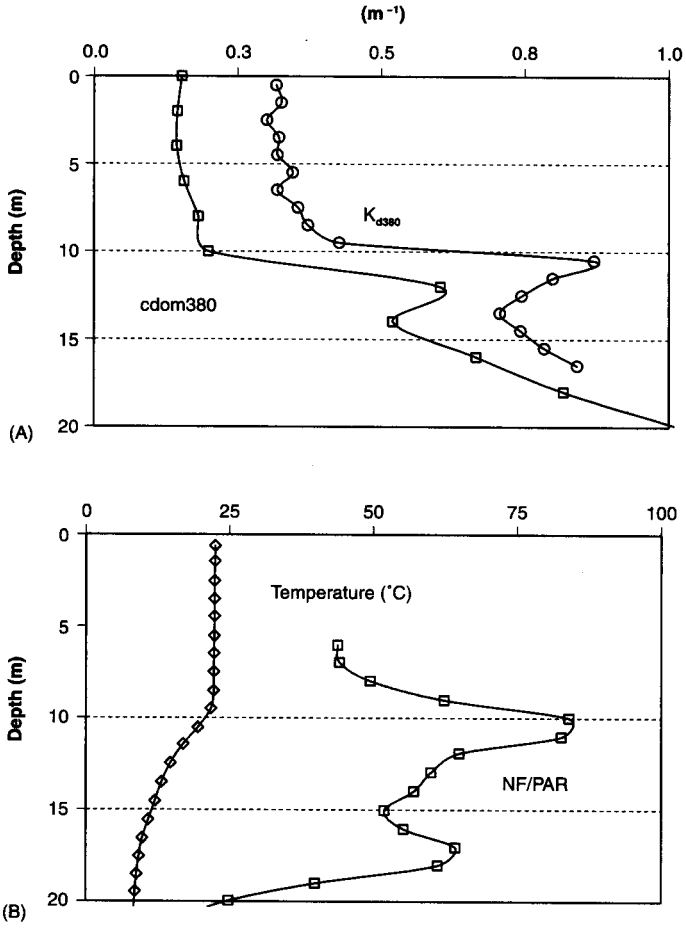

Figure 5. (A) UV-A CDOM absorption and diffuse attenuation coefficients (380 nm) for L. Giles (2 September 1999) determined using binned data from PUV-501 profiling radiometer and laboratory analysis of GF/F filtered water samples in 10 cm quartz cuvettes and Shimadzu UV160U spectrophotometer. (Hargreaves, unpublished). (B) Supplementary data from the PUV-501 profiling radiometer: water temperature and chlorophyll index (upwelling natural 685 nm fluorescence, NF, divided by downwelling PAR). In (B) The thermally mixed zone above 9.5 m corresponds to the optically mixed zone in (A). Algal biomass increases with two peaks near 10 m and 17 m that correspond to optical changes in (A) (Hargreaves, unpublished).

where ℓ is the cuvette path length (in meters). In the chemical literature the decadic absorption coefficient ($a = A/\ell$) is sometimes reported. Although the units are identical (m^{-1}), decadic units must be multiplied by 2.303 (the natural logarithm of 10) to be numerically equivalent to the standard (Napierian) exponential units from equation (12).

CDOM has an absorption spectrum that is nominally exponential in shape [4] and has been frequently characterized by the two exponential parameters,

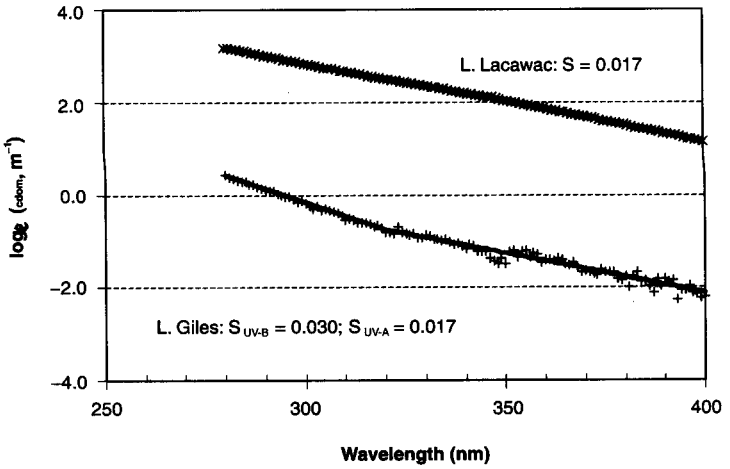

Figure 6. Spectral slope of CDOM from two lakes (Hargreaves, unpublished). S (nm^{-1}) is an exponential parameter from the relationship $\alpha_{cdom,\lambda} = ae^{-S\lambda}$. The value of S can be computed as the absolute value of the slope when $Ln(\alpha_{cdom,\lambda})$ is plotted against wavelength over the UV and blue range. Such plots tend to be linear over UV wavelengths when DOC is high (upper curve) but can sometimes be separated into a steeper UV-B slope (280–320 nm) and shallower UV-A slope (320–380 nm) when substantial photobleaching has occurred (lower curve). These lake samples are from the upper mixed layer, June 2001 (particles removed with GF/F filter, Shimadzu UV-1601 spectrophotometer, 10 cm quartz cuvette, low DOC deionized water spectrum subtracted; small glitch at 345–350 nm in lower curve is caused by spectrophotometer imperfection).

"spectral slope" (S) and reference absorption ($\alpha_{cdom,\lambda_{ref}}$):

$$\alpha_{cdom,\lambda} = \alpha_{cdom,\lambda_{ref}} e^{-S(\lambda - \lambda ref)} \tag{13}$$

where $(\lambda - \lambda_{ref})$ is the difference between the desired wavelength and the reference wavelength over the range 350–700 nm [67]. The value of S (units, nm^{-1}) is typically computed from a linear regression of $Ln(\alpha_{cdom})$ versus wavelength. The waveband used in numerous published reports has varied but frequently covers the range from UV-B through 700 nm [74]. Bricaud et al. [67] likely chose 350 nm as their lower limit after observing nonlinear regions at shorter wavelengths in their published spectra of open ocean CDOM. When α_{cdom} is high, spectra tend to be exponential from below 300 nm well into the visible spectrum (upper curve in Figure 6). At lower levels of α_{cdom}, typically following substantial exposure to sunlight, the spectra become more irregular below 350 nm. Under these circumstances, separate values for S may be calculated for the UV-B (280–320 nm) and UV-A (320–340 nm) ranges of the spectrum ([75] and K. Mopper, personal communication), as shown in the lower curve of Figure 6.

Several authors [74,76,77] have recently suggested computing S using a nonlinear regression technique that gives less weight to longer (and noisier) wavelengths. They assume that S is uniform throughout the range of wavelengths included in the nonlinear regress (otherwise the nonlinear approach would bias S toward the slope at the shortest wavelengths where α_{cdom} has the

greatest value) and they suggest that the nonlinear technique avoids a bias caused by log-transformation of instrument noise present at the longer wavelengths. This author strongly recommends the more conventional log–linear regression with a caveat to consider the following guidelines in order to compute S accurately:

- The spectrophotometer must be completely stable (e.g., warmed up for at least an hour at a stable room temperature; this is especially important with the diode array variety of instrument).
- A single carefully-cleaned quartz cuvette should be used for both blank and sample scans (referenced to air in the reference beam) with numerical correction for the blank during post processing.
- If ultrapure water is not available (stored water can develop substantial absorbance and many water purification methods leave a UV-absorbing residue) it may be preferable during post-processing to adjust the measured blanks recorded in the field with a file recorded earlier with the best quality water using the same instrument and cuvette.
- The initial selection of wavelength range for S should consider the shape of the spectrum (mentioned above).
- The baseline should be carefully adjusted to zero during post-processing at a non-absorbing waveband (e.g., 775–800 nm); this should be accompanied by visual inspection of a linear graph of α_{cdom} versus wavelength (with scales expanded to show detail, e.g., $\pm 0.05\ m^{-1}$ for the range 600–800 nm).
- The longer wavelength should be revised if necessary so as to avoid wavelengths near the instrument limit of detection (typically $A = \pm 0.001$ after subtraction of the blank and A_{base}) where noise can return negative α_{cdom} values. The effect of the baseline adjustment (described above) is to ensure that the noise is symmetrical with respect to zero, but if half the noise values are negative (and thus automatically excluded from the regression), the value of S will be underestimated to an extent that depends on how many of these "noise" data are included.

A similar exponential treatment has also been applied to spectral modeling of UV diffuse attenuation coefficients for natural waters [57,61,76] but this seems ill-advised unless the absorption spectrum of phytoplankton or other particles is insignificant or has been observed to follow the same exponential pattern as CDOM that may be present.

DOM molecules are the chemical basis for CDOM optical absorption (α_{cdom}, m^{-1}), but because of molecular variations in DOM and its chemical environment, DOC-specific absorption, (α^*_{DOC}) and DOC-specific attenuation ($K_d{}^*_{DOC}$) vary in natural waters. Both have units of $m^{-1}[g\ m^{-3}]^{-1}$, typically simplified to $m^2\ g^{-1}$. The optical properties of CDOM are known to vary with the source, including type of watershed vegetation and in situ production [6,74,78–80] and modification in the water column [22,23,74,81].

Although variation in CDOM specific absorption has been recognized for some time there is disagreement among researchers on patterns of variation with DOC concentration. Currently the scaling factor of choice is DOC concentra-

tion, rather than DOM concentration, because of standardization in methods for measuring the carbon content of DOM [40]. A linear relationship between α^*_{CDOM} and DOC has been assumed to date [23,43] in marine systems but given the pattern of variation in DOC-specific attenuation (described later), a non-linear model is proposed for DOC-specific CDOM absorption:

$$\alpha_{CDOM,\lambda} = \alpha^*_{DOC,\lambda}\, DOC^x \quad (14)$$

Values for $\alpha^*_{DOC,320}$ computed from available data (Table 2) range from 0.3 to 3.2 $m^2\ g^{-1}$ for both marine and freshwater sites (converted to 320 nm from other wavelengths as needed using reported S values and equation (13)). Data from a study of 61 lakes [60] reveal that DOC-specific absorption increases together with DOC concentration with an exponent of 1.12 and $\alpha^*_{DOC,320} = 1.2\ m^{-1}$ (Table 2). CDOM from surface waters in the Gulf of Mexico was concentrated and separated into fulvic and humic fractions [69] to indicate their relative contributions to absorption. Fulvic acids have a much lower specific absorption than humic acids. While shifting proportions of the fulvic and humic fractions in

Table 2. Variations in DOC-specific absorption of CDOM (α_1), using $\alpha_{cdom320} = \alpha_1\ DOC^x$ where units are m^{-1} for $\alpha_{cdom320}$ and $g\ m^{-3}$ for DOC concentration

$^*\alpha_1$	$^*\alpha_5$	$^\dagger x$	r^2	DOC	Region	Data from
Coastal marine DOC (extracted from Gulf of Mexico surface water)						
0.06	0.3	(1)			extracted fulvic acids	Carder et al. [69]
0.5	2.5	(1)			extracted humics	Carder et al. [69]
Coastal marine CDOM						
0.3	1.4	(1)		1.6	Japanese coastal, 13 months	Kuwahara et al. [108]
0.7	3.4	(1)		0.3–3.8	Danish coastal	Stedmon et al. [77][a]
1.3	6.5	(1)			Danish coastal	Nyquist in Højerslev [65][b]
1.9	9.5	(1)		6.2	estuarine salt marsh	Miller & Moran [109]
Coastal water receiving Delaware River discharge, comparing seasons						
2.1	10.6	(1)		0.8–1.7	Spring, water column mixed	Vodacek et al. [23]
0.6	2.8	(1)		1.3–1.5	August, surface layer	Vodacek et al. [23]
Mid-latitude lakes, comparing seasons						
1.8	9.0	(1)		0.7	Spring, L. Giles	Morris & Hargreaves [22]
0.3	1.3	(1)		1.0	Summer surface, L. Giles	Morris & Hargreaves [22]
3.2	16.0	(1)		4.4	Spring, L. Lacawac	Morris & Hargreaves [22]
1.4	7.0	(1)		5.7	Summer surface, L. Lacawac	Morris & Hargreaves [22]
Mid-latitude lake surveys						
1.2	7.4	1.12	0.79	1–24	61 Lakes, mid-latitudes	Morris et al. [60]
0.7*	10.6	1.70	0.91	4–22	30 Lakes, Northern USA	Reche et al. [115][c]
0.8	10.8	1.58	0.90	0.1–15	85 Adirondack lakes	Bukaveckas & Robbins-Forbes [24][c]

$^*\alpha_1$ is equivalent to α^*_{DOC320}; α_5 is $\alpha_{cdom320}$ computed for DOC = 5 $g\ m^{-3}$
†(1) indicated for x where a proportional scaling pattern for DOC has been assumed.
[a] TOC used to calculate specific absorption.
[b] DOM $g\ m^{-3}$ instead of DOC $g\ m^{-3}$[c]
α_1 and α_2 adjusted from 440, 340 or 300 nm to 320 nm using equation (13) and $S = 0.01565$.

the CDOM source may cause some of the variation in specific absorption of natural CDOM, other factors include changes in pH, ionic composition, and photobleaching. While the absorption by humic acids is stable over a wide range of pH (6–11), that of fulvic acids is not [82]. Stewart and Wetzel [83] studied humic substances in experimental leachate of decaying plants and DOM from 55 lakes of southwestern Michigan. They concluded that calcium concentration affects average molecular size and this in turn affects DOC-specific absorption. Vodacek et al. [23] attributed the decline in specific absorption for CDOM in the coastal plume from the Delaware River to photobleaching in the surface mixed layer. Specific absorption at 320 nm was reduced from 2.1 $m^2 g^{-1}$ during winter conditions of high river flow and low irradiance to 0.6 $m^2\ g^{-1}$ in offshore stratified surface waters during high summer irradiance (August). Morris and Hargreaves [22] observed similar declines from spring to summer in K_{d320} and $\alpha_{cdom,320}$ for several lakes differing in their CDOM source (one surrounded by a sphagnum bog, the other by well-drained soil). They established a major causal role for photobleaching through experimental exposure of particle-free lake water to different wavebands of the solar spectrum (Tables 2 and 3 and Figure 5A). In some cases a sampling artifact appears to interfere with measurements of DOC-specific absorption. In the mountain lake study by Laurion et al. [62], surface $\alpha_{cdom,320}$ was generally reduced compared to deeper in the water column, a pattern that may have been caused by photobleaching or surface inhibition of phytoplankton. However, measured $\alpha_{cdom,320}$ was greater than K_{d320} for 73% of lakes with low DOC and rocky watersheds and 21% of lakes with higher DOC and forested or meadow-covered watersheds. The authors suggested that UV-screening pigments (MAAs discussed in the next section) known to be present in the phytoplankton may have leaked out of cells during filtration. This problem might partially explain a similar anomaly in several of the 61 lakes sampled by Morris et al. [60].

CDOM exhibits fluorescence by emitting blue light after absorbing UVR. The maximum fluorescence response per unit of absorbed energy occurs when coastal CDGM is excited at 380 nm [84]. Although CDOM fluorescence is sometimes well-correlated with UV attenuation [61] and CDOM absorption [23], it has also been a somewhat variable predictor of variations in UV attenuation or absorption in other cases when the CDOM source varies [62,83]. DOC-specific fluorescence appears to vary both among and within lakes. As in the case of CDOM absorption, variations in fluorescence properties of DOC are likely to reflect differences in source as wells as a history of photochemical and biological processing. CDOM from terrestrial and marine sources can be distinguished from each other using three-dimensional excitation–emission fluorescence spectra [85,86]. McKnight et al. [80] showed that for excitation at 370 nm the CDOM emission peak of an acidified filtered water sample would occur at 442–448 nm for microbially-derived fulvic acids and at 457–461 nm for plant-derived (terrestrial) fulvic acids. Their fluorescence index (Em450 : Em500) based on these differences yielded 1.9 for microbial-derived DOM and 1.4 for terrestrial-derived DOM. This index is reported to be affected by environmental acidification, which changes DOC composition, but not by photobleaching [87].

Table 3. Relationship between $K_{d,\,CDOM}$ (m^{-1}) and DOC (g m^{-3}) using $K_{d320} - K_{w320} = k_1\,DOC^x$; Published K_{d320} and DOC data were used with $K_{w320} = 0.04$ to fit k_1 and x (least squares regression) where $k_1 = K_{CDOM,\,320}$ at DOC = 1 g m^{-3} and $k_5 = K_{CDOM,\,320}$ at DOC = 5 g m^{-3}

k_1	k_5	x	r^2	DOC	Region	Data from
Coastal & Marine						
1.3	7	(1)			Ocean (based on DOM)	Højerslev [65]
0.8[a]	4[a]	(1)		2.5	St. Lawrence Estuary, Stn 24	Kuhn & Browman [57]
0.4		(1)		1.7	Coastal Japan, 8 m. w/rain	Kuwahara et al. [108]
0.2		(1)		1.5	Coastal Japan, 5 m. dry	Kuwahara et al. [108]
43 Canadian prairie lakes, ponds, wetlands, including saline systems						
6.7[a]	18[a]	0.61	0.41	24–80	52°N Wetlands, ponds	Arts et al. [34][b]
1.4[a]	5	0.76	0.50	4–156	52°N Lakes	Arts et al. [34][b]
Freshwater: photobleaching effects in surface waters of lakes						
2.0		(1)	0.7		41°N, L. Giles, spring	Morris & Hargreaves [22]
0.3		(1)	1		41°N, L. Giles, summer	Morris & Hargreaves [22]
	19	(1)	4.4		41°N, L. Lacawac, spring	Morris & Hargreaves [22]
	9	(1)	5.7		41°N, L. Lacawac, summer	Morris & Hargreaves [22]
Freshwater: lakes differing in land cover and altitude						
0.6	3[a]	0.89	0.54	0.2–1	Alps & Pyr., rocky	Laurion et al. [62][c]
1.4	7[a]	0.81	0.68	0.4–4	Alps & Pyr., trees, meadows	Laurion et al. [62][c]
1.0	8[a]	1.33	0.81	0.2–4	Alps & Pyrenees, combined	Laurion et al. [62][c]
Freshwater: high latitude lakes						
0.3	10	2.08	0.93	0.3-11	Arctic, subArctic, Antarctic	Vincent et al. [68]
0.3	13[a]	2.43	0.99	0.3–1	Antarctic	Vincent et al. [68]
0.4[a]	10	2.06	0.86	2–11	Sub-Arctic Canada	Laurion et al. [61]
0.7[a]	10	1.62	0.78	4–11	Alaska, USA	Morris et al. [60][d]
0.8	6	1.28	0.97	1–5	Arctic Canada	Laurion et al. [61]
Freshwater: mid-latitude lakes						
0.6	7	1.62	0.91	0.5–8	41–51°N. USA & Canada	Scully & Lean [33][d]
0.6	7	1.57	0.90	1–24	41° N Pennsylvania,USA	Morris et al. [60][d]
1.7	13[a]	1.24	0.78	0.4–3	40°S, Argentina	Morris et al. [60][d]
3.1	12	0.83	0.60	0.8–10	Colorado, USA	Morris et al. [60]
1.5	10	1.20	0.84	0.4–24	Average, mid-latitudes	Morris et al. [60][d]

[a] k_1 or k_5 extrapolated beyond measured range of DOC.
[b] Waveband used for K_d was UV-B (280–320 nm) instead of narrow-band 320 nm.
[c] Excluding lakes when $C/L > 50$ (C = catchment area, L = lake area).
[d] Excluding data when DOC low relative to phytoplankton (DOC/chl < 1400, units, g m^{-3}).

Figure 7 shows the emission spectrum of CDOM fluorescence for samples excited at 365 nm from two lakes having DOC in the range of 1–5 mg l^{-1} (Hargreaves, unpublished). The small peak is Raman scattering by water molecules (centered at 417 nm, a shift in wavenumber of -3400 cm^{-1} from the excitation wavenumber, where wavenumber is 10^7 divided by wavelength in nm). The Raman water peak can be used to provide scale calibration of fluorescence emission spectra [88,89]. The broad peak in Figure 7 is contributed predominantly by the fulvic acid fraction of DOM [80]. The peak wavelength and

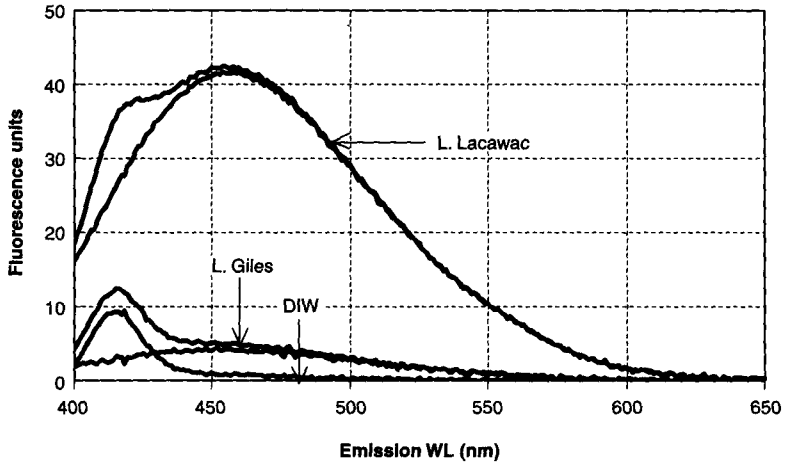

Figure 7. CDOM fluorescence of water from two lakes (Hargreaves, unpublished): emission scans for excitation at 370 nm (Shimadzu 551 fluorometer), before and after subtraction of water blank. Samples: deionized water (DIW), L. Giles water (ca. 1 g m^{-3} DOC), L. Lacawac water (ca. 5 g m^{-3} DOC) The Raman scattering peak at 417 nm represents a shift in wavenumber by 3400 cm^{-1} from the excitation wavenumber. The broad peak is contributed predominantly by the fulvic acid fraction of DOM. The peak wavelength and fluorescence index ratio for these samples (L. Giles, 452 nm peak and ratio = 1.5; L. Lacawac, 455 nm peak and ratio = 1.4) suggest a slight difference in CDOM source [80].

fluorescence index ratio for these samples (L. Giles, 452 nm peak and ratio = 1.5; L. Lacawac, 455 nm peak and ratio = 1.4) suggest a slight difference in CDOM source.

Values for $K_d{}^*_{DOC,320}$ ranging from 0.3 to 3.8 (Table 3) have been calculated from published UV attenuation data for both marine and freshwater sites (converted into 320 nm as needed using reported S values and equation (14)). The attenuation of pure water was subtracted ($K_{w,320}$ discussed below) and sites with high chlorophyll relative to DOC (DOC/chl < 1400; units g m^{-3}) were excluded where noted. Although some K_d's may be elevated by phytoplankton and other particles that attenuate underwater irradiance, the predominant source of variation in $K_d{}^*_{DOC,320}$ is DOC quality. While Scully and Lean [33] reported no effect of phytoplankton in their optical model (chlorophyll ranged from 1.3–33 mg m^{-3}), a reassessment shows that when lakes with a low ratio of DOC to algal chlorophyll (DOC/Chl < 1400; units g m^{-3}) were excluded, there was an improved r^2 for the regression of K_d versus DOC and a reduced K^*_{DOC}. The regressions of Morris et al. [60] were also improved by reanalysis in which lakes with low DOC/Chl ratios were excluded, although only three lakes (out of 64 sampled) had chlorophyll levels exceeding 5 mg m^{-3}.

A linear model for scaling $K_d{}^*_{DOC,320}$ to DOC concentration was adopted by Baker and Smith [43], who used a constant value of $K_d{}^*_{DOC,320} = 1.3$ in their bio-optical model but cited a range of values from as low as $K^*_{DOC,320} = 0.75$ for

clear Sargasso Sea water to as high as $K^*_{DOC,320} = 6.2$ for a coastal site. A linear relationship between K^*_{DOC} and DOC has been assumed in several studies [61,62]. A power relationship between K^*_{cdom} and DOC (similar to that describe for CDOM absorption above) has been assumed by others:

$$K_{d,cdom,320} = K^*_{DOC,320}\,DOC^x \tag{15}$$

where $K^*_{DOC,320}$ is the DOC-specific attenuation of CDOM at 320 nm.

The power model for relating UV attenuation to DOC was used by Scully and Lean [33], Morris et al. [60] and Vincent et al. [68]. Vincent et al. [68] found an unusually strong relationship between UV attenuation depths and DOC for high-latitude lakes (replotted in Figure 8 as $K_{d320} - K_{w320}$ versus DOC), a relationship with an exponent much greater than one. Arts et al. [34] used both linear and power models (but preferred the power relationship) to relate wide-band UV-B attenuation to DOC in prairie lakes of Canada. As reported by Arts et al. [34] a reasonable fit was obtained with a power model, but when all ponds and wetlands are grouped (including three with high salinity), they have exponents less than one, similar to the fresh and saline lakes (Table 3). While attenuation for the UV-B waveband (derived from detailed spectral irradiance) is too broad to serve as a rigorous attenuation coefficient, it is an index of K_{d320} that is largely a function of DOC concentration and quality. Although Arts et al. [34] concluded that UV-B irradiance penetrates more deeply into saline water bodies that it does into freshwater systems of similar DOC concentration, this reanalysis of their data supports a somewhat contrary conclusion (Figure 9). Saline systems tend to have higher [DOC] than freshwater systems (probably because evaporation causes DOC to become more concentrated). For similar [DOC], the greater penetration is actually observed in lakes (especially the large,

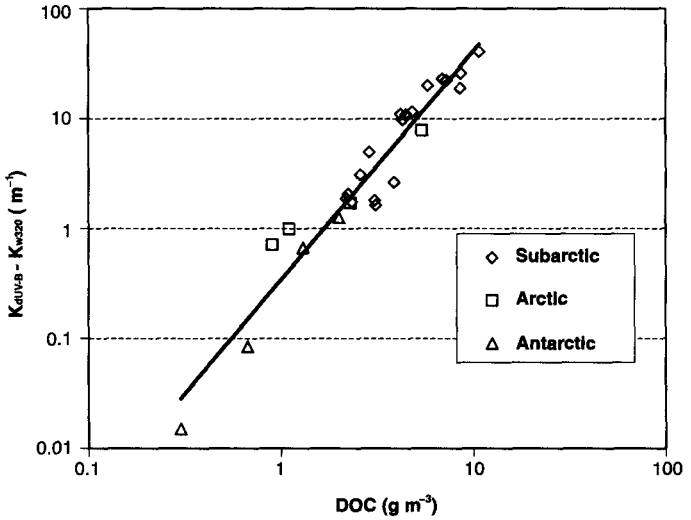

Figure 8. Lake data computed from Vincent et al. [68] to show the power relationship between $(K_{d320} - K_{w320})$ and DOC concentration for a range of high latitude lakes. The equation for all sites combined is $(K_{d320} - K_{w320}) = 0.34DOC^{2.08}$ ($r^2 = 0.93$).

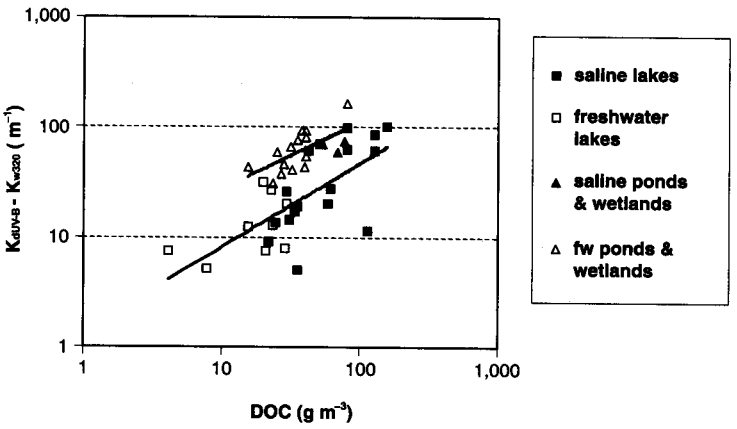

Figure 9. Attenuation of UV-B irradiance in saline prairie lakes, ponds, and wetlands of Canada (52°N) from Arts et al. [34]. Saline systems tend to have higher [DOC] than freshwater systems (probably because evaporation causes DOC to become more concentrated). For similar [DOC], greater penetration of UVR is observed in lakes (especially the large, deep ones) compared to small and shallow ponds and wetlands. The equation for all ponds and wetlands (triangle symbols) is $K_{dUV\text{-}B} = 6.7\ DOC^{0.61}$ ($r^2 = 0.41$); for freshwater ponds and wetlands (open triangles) $K_{dUV\text{-}B} = 2.5\ DOC^{0.91}$ ($r^2 = 0.56$); for all lakes (squares), $K_{dUV\text{-}B} = 1.4\ DOC^{0.76}$ ($r^2 = 0.50$).

deep ones) compared to small and shallow ponds and wetlands. Arts et al. [34] noted this pattern and hypothesized that attenuation is lower per unit of DOC in deep lakes because their greater residence time allows for more complete photobleaching. Waiser and Robarts [90], studying one of these large lakes, found lower [DOC] but higher UV-B attenuation per unit of DOC in a major stream feeding the lake compared to the lake water column. Although salinity covaries with DOC in xeric regions such as this, it is a weak predictor of UV-B attenuation because DOC-specific attenuation also varies.

3.3.2 Role of phytoplankton and CDOM (Kirk type A and GA natural waters)

Phytoplankton can contribute significantly to UV attenuation in waters with moderate to low UV attenuation, especially when isolated from watershed sources of CDOM. In Case 1 oceanic waters where coastal discharge is not a source of CDOM [52] the levels of locally-produced DOC, algal pigments, and the associated microbial community are assumed to co-vary [43,58] but perhaps with a time delay between algal production and appearance of CDOM [67,69,85,91]. It can be difficult to establish the indirect contribution of phytoplankton to water column optics by their release of DOM which increases α_{cdom}. For example, the spatial correlation between a peak in α_{cdom} just below the mixed layer of a lake (Figure 5A) and a peak in abundance of phytoplankton at the same depth (Figure 5B) are suggestive of a causal relationship, but not definitive.

Studies of optical properties of photosynthetic organisms are numerous, but relatively little has been published on the role of UV attenuation by phytoplankton. Blough and Del Vecchio [74] summarize spatial and temporal relationships between CDOM, DOC and phytoplankton in coastal waters. Belzile et al. [49] report data from L. Biwa, Japan, in which both α_{cdom} and [chl *a*] (over the range 1.5–7.5 mg m^{-3}) are highly correlated with K_{d320} and K_{d380}. Twardowski and Donaghay [116] inferred from optical measurements at a coastal site the direct production of CDOM from a thin layer of phytoplankton in the water column.

A key parameter in bio-optical models is the chlorophyll-specific spectral absorption factor ($\alpha^*_{Chl,\lambda}$). Chlorophyll concentration is most often measured optically after extraction from phytoplankton. In vivo methods involving measurement of fluorescence can provide a convenient index of biomass but are confounded with acclimation and species effects on calibration parameters. The Quantitative Filter Technique (QFT) is widely used to provide a measure of particulate absorption over the waveband (typically 400–700 nm) of photosynthetically active radiation (PAR). The method, pioneered by Yentsch [53], involves concentrating particles onto a filter and then measuring absorption on the filter in a spectrophotometer. Many workers have contributed to refining this method; Kishino et al. [54] added an option to estimate separately the contribution of photosynthetic pigments and detritus by extraction with hot methanol, while Mitchell [55,56] established a standard technique and then extended it to different instruments and filter types. Numerous modifications to the QFT have been proposed (most recently by Roesler [92], Lohrenz [51] and Tassan et al. [93]) because of complications with calibration and the effects of loading and particle type. The QFT is the basis for a recent review by Morel [58] summarizing systematic variation in $\alpha^*_{Chl,PAR}$ of marine phytoplankton: the values are lowest in eutrophic waters and highest in oligotrophic waters. Over the chlorophyll range from 0.03 to 30 mg m^{-3} the value of α^*_{Chl} decreases by a factor of 10. He attributes roughly half of this variation to changes in cell size, and half to changes in accessory pigments, but does not address the issue of UV absorption. A new technique involving water column profiles made with an in situ absorption instrument (WET Labs, Inc. AC-9) is revolutionizing the characterization of α_{phyto} in visible wavelengths by allowing in vivo IOP measurements of phytoplankton and associated optical constituents at nine wavelengths (e.g., [49]). When a pair of instruments is lowered together, one can record absorption and beam attenuation at nine visible wavelengths for whole water while simultaneously recording the same signals for particle-free water [30].

The QFT can be used to measure UV absorption of particles, including phytoplankton cells, if the samples are analyzed shortly after filtering [47]. Figure 10 shows summer near-surface particulate absorption spectra for three lakes with different chlorophyll *a* and DOC concentrations (Hargreaves, unpublished). Comparing the three lakes, Crater Lake near-surface waters have the lowest concentrations of DOC (<0.2 g m^{-3}, [94]) and chlorophyll *a* (<0.2 mg m^{-3}, Emmanuel Boss, personal communication). Lake Giles is intermediate (1.1 g m^{-3} and 0.6 mg m^{-3}), and L. Lacawac has the highest concentrations

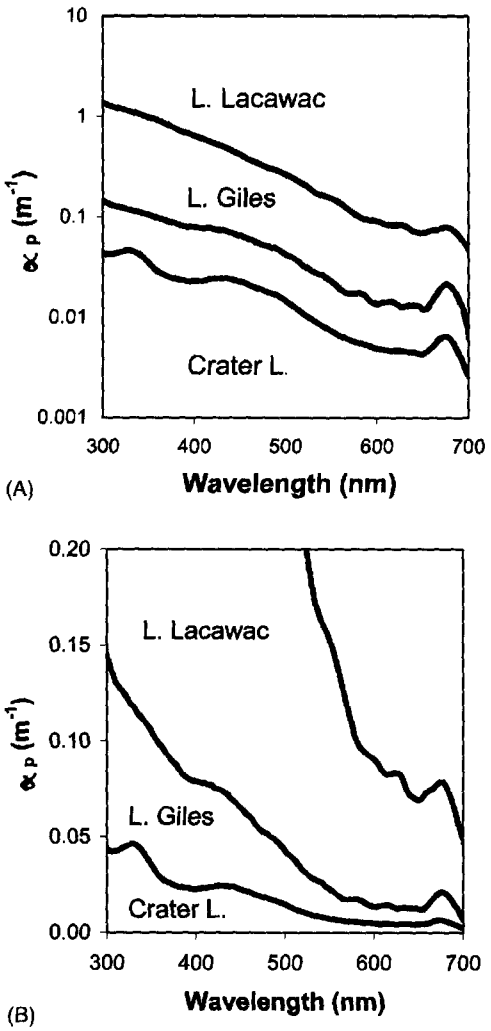

Figure 10. Particulate absorption for three lakes with different chlorophyll *a* and DOC concentrations (Hargreaves, unpublished). Crater L conditions: August 2001, Depth 25 m, $K_{d320}=0.066$. Typical late summer near surface DOC < 0.2 g m^{-3} and chl-*a* <0.2 mg m^{-3} ([94], and Emmanuel Boss, personal communication). L. Giles conditions: June 2001, depth 0–6 m; DOC $=1.1$ g m^{-3}, chl-*a* $=0.6$ mg m^{-3}, $\alpha_{cdom320}=0.48$ m^{-1}, $K_{d320}=0.68$ m^{-1}. L. Lacawac conditions: June 2001, Depth, 0–2 m; DOC $=4.7$ g m^{-3}, chl-*a* $=2.7$ mg m^{-3}, $\alpha_{cdom320}=12.3$ m^{-1}, $K_{d320}=14.9$ m^{-1}. QFT method from Mitchell [56] as adapted by Roesler [92] using GF/F filters supported on quartz discs in a Shimadzu UV-1601 spectrophotometer. (A) Log scale. (B) Linear scale. The spectra for L. Lacawac ($\alpha_{p320}=1.2$ m^{-1}, $\alpha_{p675}=0.08$ m^{-1}) and L. Giles ($\alpha_{p320}=0.12$ m^{-1}, $\alpha_{p675}=0.02$ m^{-1}) show the blue and red peaks for chlorophyll superimposed on a CDOM-like exponential pattern of particulate absorption. Crater L. ($\alpha_{p320}=0.045$ m^{-1}, $\alpha_{p675}=0.006$ m^{-1}) shows a spectrum of algal pigments with a peak at 330 nm in addition to typical blue and red chlorophyll peaks. Crater L. chlorophyll *a* at 25 m depth calculated from the 675 nm peak (proportional to the other lakes) is 0.18–0.20 mg m^{-3}.

(4.7 g m^{-3} and 2.7 mg m^{-3}). In L. Giles and L. Lacawac the value for chlorophyll-specific absorption at 675 nm ($\alpha^*_{chl,675}$) is 0.03 from these data. The spectra for L. Lacawac ($\alpha_{p320} = 1.2\ m^{-1}$, $\alpha_{p675} = 0.08\ m^{-1}$) and L. Giles ($\alpha_{p320} = 0.12\ m^{-1}$, $\alpha_{p675} = 0.02\ m^{-1}$) show the blue and red peaks for chlorophyll superimposed on a CDOM-like exponential pattern of particulate absorption. Crater L. ($\alpha_{p320} = 0.045\ m^{-1}$, $\alpha_{p675} = 0.006\ m^{-1}$) shows a spectrum of algal pigments with a peak at 330 nm in addition to typical blue and red chlorophyll peaks.

Figure 11 shows underwater spectral irradiance in Crater Lake, OR (Hargreaves, unpublished). Data were collected during continuous lowering of two radiometers from 13:20–14:30 local time, 20 August 2001 (solar zenith angle 31–36°, clear sky) using a PRR-800 multichannel reflectance profiling radiometer to 153 m and a PUV-2500 profiling UV radiometer to 60 m. These filter-band radiometers have a sensor bandwidth of 8–10 nm and can rapidly and accurately track downwelling cosine irradiance (and upwelling radiance, in the PRR-800) over more than 7 decades of intensity. (Biospherical Instruments, Inc.). The PRR-800 was similar to the unit used for Figures. 1 and 2, but was equipped to sense a slightly different set of sensor wavebands (both PRR-800's included 340 and 380 nm channels). The PUV-2500 has sensors for downwelling cosine irradiance centered at 305, 313, 320, 340, and 380 nm and PAR and for upwelling 683 nm radiance (not shown). The hybrid spectrum in Figure 11 combines

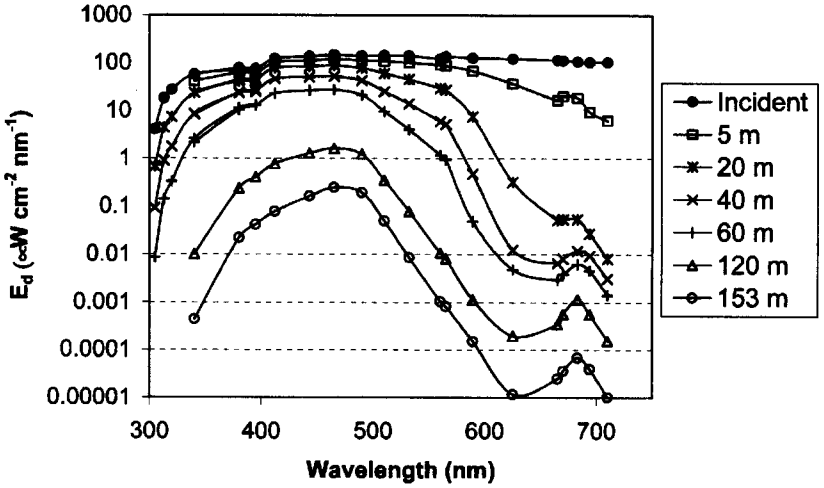

Figure 11. Crater Lake, Oregon: Underwater spectra of downwelling cosine irradiance with very low CDOM and algae concentrations, especially in the surface waters above 20 m. Data collected during continuous lowering from 13:20–14:30 local time, 20 August 2001 (solar zenith angle 31–36°, clear sky) using a PRR-800 multichannel reflectance profiling radiometer to 153 m and a PUV-2500 profiling UV radiometer to 60 m (8–10 nm bandwidth sensor response, Biospherical Instruments, Inc.). This hybrid spectrum using depth-binned data (with overlap at 340, 380, and 395 nm) is plotted on a log scale to show a range of irradiance spanning seven decades of magnitude. Except for the peak around 685 nm (caused by algal fluorescence), deep irradiance at WL > 520 nm likely was caused by Raman scattering from shorter wavelengths.

depth-binned data from both instruments for 20, 40, and 60 m (overlap from the two instruments is visible at 340, 380, and 395 nm) on a log scale to show a range of irradiance spanning seven decades of magnitude. Except for the peak around 685 nm (caused by algal fluorescence), deep irradiance at WL >520 nm likely was caused by Raman scattering from shorter wavelengths. At these longer wavelengths accurate estimates of K_d are restricted to high-irradiance surface waters. Compared to Figure 1, the shorter wavelengths penetrate much more deeply in Crater Lake (in the coastal water at 40 m the irradiance at 340 nm is similar to that at 153 m in Crater L.). As was the case in Figure 1, the red peak caused by algal fluorescence is visible at all depths but the relative magnitude of the red peaks are different.

Figure 12 shows spectral K_d for Crater Lake calculated at 10 nm intervals from underwater spectral irradiance data collected at nearly the same time as the data in Figure 11, in this case using a LI-COR spectroradiometer (model LI-1800UW, 8 nm bandwidth). Spectral values for $K_{w,\lambda}$ (freshwater) estimated by Smith and Baker [18] are also included for comparison, and two new estimates of $K_{w,\lambda}$ that will be discussed in section 3.3.4. LI-COR $K_{d,\lambda}$ values for Crater Lake have been replicated using PRR-800, PUV-501, and PUV-2500 instruments (Biospherical Instruments, Inc.) on several dates. The accuracy of the LI-COR and PUV-501 instruments for measuring UV diffuse attenuation has

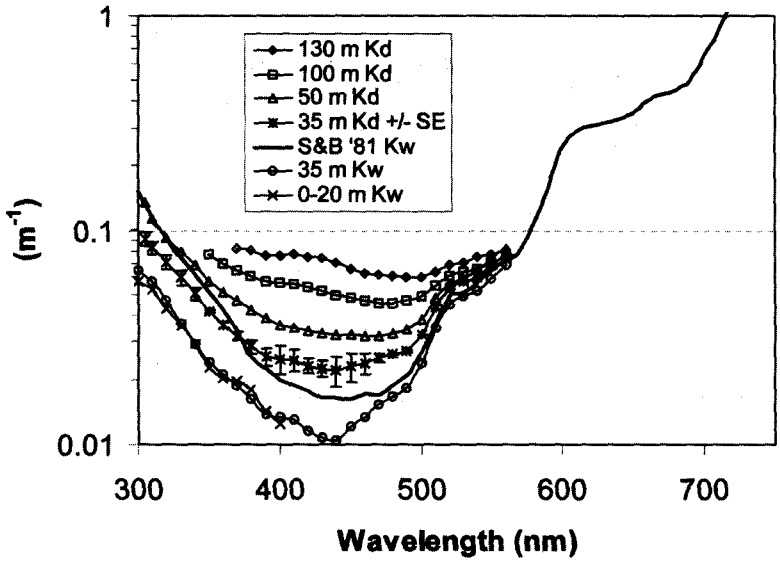

Figure 12. Spectral diffuse attenuation coefficients ($K_{d,\lambda}$) calculated at 10 nm intervals for Crater Lake Oregon, from downwelling irradiance scans at fixed depths, 12:00–13:00 local time, 20 August 2001 (SZA = 31°, clear sky) using a LI-COR LI-1800UW spectral radiometer (8 nm bandwidth single monochromator). $K_{w,\lambda}$ for freshwater estimated by Smith and Baker [18] is also compared to two new estimates computed by subtracting particulate absorption (measured similarly to spectra in Figure 10) from $K_{d,\lambda}$ averaged over 0–20 m and 30–40 m, adjusted for sky and sun angle (Figure 4B).

also been demonstrated in a field comparison [36]. Details of Crater Lake UV attenuation data will be published separately (B. Hargreaves, G. Larsen, J. Morrow, and others).

In Crater Lake during August, phytoplankton are extremely scarce in the upper 15 m (chlorophyll concentration ca. 0.1–0.2 mg m^{-3} [94 and Emmanuel Boss, personal communication]), a depth that also represents $Z_{37\%}$ for 320 nm. Typically the Crater Lake chlorophyll concentration in August increases with depth to a maximum concentration near 130 m (ca. 0.6 mg m^{-3} [94 and Emmanuel Boss, personal communication]). As the phytoplankton pigment increases with depth, the phytoplankton optical effects (direct and via CDOM) on UV and PAR diffuse attenuation increase as well (Figure 12). By comparing the curves for K_{d320} and K_{w320} in Figure 12 it is apparent that phytoplankton and associated CDOM absorption are contributing about 50% of the diffuse 320 nm attenuation at 50 m ($K_{d320}=0.092$ m^{-1}, $K_{w320}=0.045$ m^{-1}). Ayoub et al. [46] used the QFT to determine relative importance and seasonal variations for UV absorption by phytoplankton in the two lakes represented in Figure 10. The contribution of particulates was also high for oligotrophic L. Giles (particles contributed 20–55% of total absorption at 320 nm) but was low for the humic L. Lacawac (8–18% of total absorption, with particles dominated by CDOM-like detritus rather than phytoplankton). Other cases of within-lake variation in UV attenuation attributed to phytoplankton include high mountain lakes [62,63] and Lake Biwa, Japan [49]. More work will be required to determine if depth-variation in phytoplankton biomass and in chlorophyll-specific absorption represent the same biotic mechanisms and range of values reported for horizontal trophic gradients in ocean waters [58] and among lakes.

Absorption in the UV-A wavelengths includes accessory pigments associated with photosynthesis while UV-B absorption by living cells is caused in part by proteins and nucleic acids. Compounds that absorb with various peaks in the UV range accumulate in some organisms subject to UVR exposure and may serve as UV-B screening compounds: myco-sporine-like amino acids (MAA's) in algae and invertebrates and scytonemin and its derivatives in cyanobacteria [45,50, Chapter 10]. Chlorophyll-specific absorption is known to change with depth in the water column, but while the specific absorption of photosynthetic pigments tends to increase in dim light as depth increases, the response of UV-screening pigments may be opposite. Helbling et al. [44] adapted the QFT to measure UV and visible chlorophyll-specific absorption by marine phytoplankton (α^*_{Chl}) in marine waters of Antarctica and observed a UV-protective pigment whenever algae were exposed to at least 1% of incident UV-B (320 nm) irradiance. They observed a UV absorption peak between 310 and 330 nm for algae within the upper mixed layer as deep as 20 m (roughly the $Z_{1\%}$ attenuation depth for 320 nm) and down to 90 m when thermal stratification was weak enough to allow deep mixing. The value for α^*_{Chl} at 327 nm varied inversely with the depth of the mixed layer for a large number of samples, especially when diatoms were dominant, suggesting that some algae produce a UV screening pigment in proportion to their UV-B exposure. A similar UV-B particulate absorption peak was observed in Crater Lake, Oregon above the $Z_{1\%,320}$ depth

(Hargreaves, unpublished). In this case the peak was evident at 50 m (Figure 10), but not at 100 m, when the mixing depth was approximately 10 m and $Z_{1\%,\,320}$ was 60 m (Figure 11).

3.3.3 Ultra-low attenuation (Kirk type W, WA, or WG natural waters)

Early studies of UV attenuation identified several ocean regions as unusually transparent. Table 1 shows three regions (Sargasso Sea, East Mediterranean, and central equatorial Pacific) with $K_d \leq 0.15$ in the range of 310–320 nm, including the earliest radiometer measurement of underwater UV-B attenuation [95]. Crater Lake Oregon is the only freshwater site to receive early attention for its "near distilled water" transparency near the surface. Crater Lake spectra for visible (Tyler [96]) and UV-A (Smith and Tyler [97]) wavelengths were recorded by the first underwater scanning spectroradiometer (Tyler and Smith [98]). An improved instrument recorded UV-A and visible spectral irradiance underwater in Crater Lake during July 1969 [99]. The authors commented on the similarities of Crater Lake water optical properties to those of pure water. There are no published data for Crater Lake using later versions of the spectroradiometer [8,100] that included the capacity to record UV-B wavelengths.

In the 1990's new commercial UV instruments made possible a large number of lake measurements, with the result that high mountain lakes in Austria, North America, and South America have been identified with $K_{d320} \leq 0.17$ (Table 1). Vincent et al. [68] measured UV attenuation in several Antarctic lakes and reported record low values for the depth range 10–20 m below the ice-covered surface of Lake Vanda ($K_{d320} = 0.055$), values smaller than the attenuation estimated for pure water reported by Smith and Baker [18]. Recent UVR measurements at Crater Lake OR revealed similar low values in surface waters (K_{d320} from 0.050 to 0.071, Table 1). As indicated by equation (10), K_d values include contributions from water, phytoplankton, and DOC. These recent low values for two lakes suggest that CDOM and phytoplankton concentrations are very low. The implication that the Smith and Baker's [18] values for K_w are too high in the UV wavelengths will be addressed in the next section. In both Crater Lake and Lake Vanda, UV attenuation changes with depth and is minimal near the surface. From the limited information available it appears that both phytoplankton and CDOM contribute to this change in UV attenuation with depth, as discussed in the previous section.

At Crater Lake, DOC levels have been reported to be less than 16 μM (equivalent to 0.2 mg l^{-1}) with algal biomass in surface waters <0.2 mg m^{-3} chlorophyll [94 and Emmanuel Boss, personal communication]. At Lake Vanda, DOC in the UV-transparent surface water is reported to be 0.3 g m^{-3} with algal biomass <0.1 mg m^{-3} chlorophyll [68]. The role of CDOM at such low attenuation levels is difficult to measure by spectrophotometer and even the concentration of DOC is at the level of "blank" values for high temperature oxidation instruments [40]. If one assumes that the surface value for DOC in Crater Lake is actually 0.2 g m^{-3} at the time of low K_d measurements, the

absorption by CDOM can be estimated using the DOC specific absorption relationship published for other sites. Marine DOC concentrated from Gulf of Mexico and Mississippi River plume water by Carder et al. [69] would give $\alpha_{cdom320} = 0.02\ m^{-1}$ if all the DOC consisted of marine-like fulvic acids (equivalent to $\alpha_{cdom,412} \approx 0.001$), or $\alpha_{cdom320} = 0.11\ m^{-1}$ if it were all marine-like humic acids. The lower estimate, $0.02\ m^{-1}$ at 320 nm, could be a component of the minimum K_{d320} value in Crater Lake of $0.05\ m^{-1}$, depending on the absorption and scattering attributed to water molecules and phytoplankton. Using the reported DOC value of $0.3\ g\ m^{-3}$ for Lake Vanda surface waters, the predicted K_{d320} is $0.035\ m^{-1}$ (again, assuming marine-like fulvic acids), compared to measured $K_{d320} = 0.055\ m^{-1}$. K_{d320} can also be estimated using a regression of K_{d320} versus DOC from a series of high latitude lakes (Figure 8) that included Lake Vanda and other Antarctic lakes ([68] and Table 3). Predicted K_{d320} ranges from 0.060 to $0.090\ m^{-1}$ for lakes with DOC in the range 0.2–0.3 mg l^{-1} (after adding $K_{w320} = 0.04$). To avoid introducing a latitudinal bias (caused by sun angle differences) future relationships of this sort should be adjusted using equation (11).

3.3.4 Attenuation and absorption by pure water

The extremely low UV attenuation in surface waters of Crater Lake provides an opportunity to improve the Smith and Baker [18] "upper bounds estimate" of UV attenuation in pure water, K_w. The recent near-surface measurements of spectral K_d (Figure 12) and spectral absorption of particles (Figure 10) can be combined to make a new "upper bounds estimate" of K_w. Spectral $K_{w,\lambda}$ values averaged over depths of 0–20 m and 30–40 m are shown in Figure 12, along with the freshwater K_w spectrum from Smith and Baker [18]. The new "K_w" estimates have been computed by first adjusting K_d's with equation (11) for diffuse and direct sunlight (see Figure 4B) and then subtracting particle absorption appropriate to the depth. Because of uncertainties with the QFT calibration for this lake, the particulate absorption values were adjusted downward from the values calculated by the Roesler method [92] until the two estimates of spectral K_w (0–20 m and 30–40 m) converged. The final adjustment was to 37% of the original particulate absorption coefficient values. A justification for this approach is that unpublished measurements of α_{cdom} made several weeks later by Emmanuel Boss (personal communication) using a Wetlabs AC-9 in situ absorption meter showed $\alpha_{cdom440}$ essentially uniform in the top 40 m and just above the limit of detection for the instrument. Another supporting argument is that the same adjustment improves an estimate for chlorophyll *a* concentration at 25 m depth calculated from the particulate absorption peak at 675 nm (Figure 10). By using $\alpha^*_{chl,675} = 0.012$ derived from September data (2001 AC-9 particle absorption and extracted chlorophyll *a* concentration; Emmanuel Boss, personal communication), the uncorrected estimate for chlorophyll *a* concentration ($0.5\ mg\ m^{-3}$) was reduced to a reasonable value within the normal range for that depth in Crater Lake ($0.18\ mg\ m^{-3}$). Tassan et al. [93] have suggested that small

phytoplankton (such as those abundant in the surface of Crater Lake) cause the Roesler method [92] to overestimate particulate absorption. The resulting "K_w" estimates may still include scattering effects of particles present plus absorption by any cdom present that was not correlated with particle absorption. For UV wavelengths the Crater Lake "high" estimates for K_{w320} from 0–20 m and 30–40 m range from 0.043 to 0.047 m^{-1}. These are substantially lower than the Smith and Baker [18] value of $K_{w320}=0.09$ m^{-1}. Note that these freshwater values of $K_{w,\lambda}$ from Smith and Baker [18] include slightly smaller backscatter terms than the seawater $K_{w,\lambda}$ values used in Figure 2.

A laboratory study of spectral absorption by pure water [101], which extended only into the UV-A wavelengths, reported pure water absorption as $\alpha_{w380}=0.011$ m^{-1}. This value can be converted into K_{w380} using equation (9) (with $b_{bw380}=0.007$ from Mobley [5]) to yield $K_{w380}=0.017$ m^{-1}, compared to the Crater Lake estimate, $K_{w380}=0.018$ m^{-1} (using near surface K_{d380} averaged from several instruments, August 2001). Both values are lower than the Smith and Baker [18] estimate, $K_{w380}=0.026$. Further refinements in estimates for spectral K_w and α_w for UV wavelengths could result from improved measurements of spectra for K_d, particle absorption, CDOM absorption, and particle scattering in the remarkably clear waters of Crater Lake.

3.4 Predicting levels of UV-attenuating constituents

A range of bio-optical models (described in Section 3.3) can be used to estimate UV attenuation in natural waters when the concentrations and optical properties of algal pigment and DOC are known. How can these concentrations and optical properties be predicted from regional-scale features of the environment? Predicting typical concentrations and optical properties for either algal pigments or DOC in an aquatic system will require knowledge about sources and sinks, mechanisms for changing optical properties, and how each of these responds to the environment, a subject that will be only briefly reviewed here. Only passing mention will be made here of the role of inorganic particles, which can be extremely important as UV attenuators in some aquatic systems [6, 10, 49]. Such systems are shallow or subject to erosion: streams and rivers with disturbed or non-vegetated watersheds, and shallow lakes or coastal systems where the high energy keeps particles suspended in the water column. One special case is the precipitation of carbonates that imparts a whitish color (observed in several lakes by Laurion et al. [62]). Another special case is the meltwater from glaciers, where interactions with the underlying rock surface create small particles that give the water a milky appearance.

Phytoplankton abundance responds to nutrients, light, and grazing pressure. The primary autochthonous source of CDOM is often assumed to be photosynthetic organisms, but heterotrophic bacteria may play an important role by processing the relatively UV-transparent photosynthate and releasing modified compounds that absorb UVR more strongly [91]. Spatial and temporal linkage between CDOM and the microbial community appears complex and difficult to

predict at present, in part because the microbial community also attenuates UVR. Predictions about microbial UV attenuation are rather difficult at present because there are so few measurements and reliability of current techniques (e.g. QFT) is still being debated. The adaptive physiological and evolutionary responses of phytoplankton to UVR are likely to differ from their adjustments of photosynthetic pigments to light and depth. Here again there is too little information to make predictions except that one should not be surprised to find UVR screening pigments in phytoplankton exposed to high UVR (perhaps when 320 nm irradiance exceeds 1% of surface levels?).

The balance between sources and sinks for DOC will determine its concentration in natural waters and thus establish a major factor in UV attenuation. The levels and optical properties of CDOM in aquatic systems will depend in part on whether the source is within the water column (autochthonous) or coming from elsewhere (allochthonous). Allochthonous sources include watershed runoff (e.g. from soil or wetlands, especially water-saturated soils but also from man-modified surfaces which may be enriched with petroleum hydrocarbons), and wastewater discharge. In estuaries the large CDOM load typically carried by rivers is both diluted (and to a lesser extent, precipitated) as it mixes with brackish water. Allochthonous sources are affected by precipitation, evaporation, soil hydraulic residence time, and temperature, which influence production of CDOM in saturated soils and transfer, dilution, and concentration of this material in receiving waters. In a comparative study of 337 lakes from northern USA and Canada, Rasmussen et al. [102] found a strong positive correlation between CDOM and the ratio of drainage area to lake area, and a negative correlation between CDOM and average slope of the drainage landscape. CDOM in coastal regions is strongly correlated with river discharge and inversely correlated with salinity [74]. CDOM in two Australian reservoirs was highly correlated with season, increasing during rainy periods and declining during dry, sunny periods in response to microbial and photochemical degradation [103]. The two reservoirs differed in average level of CDOM, with 97% of the variability in average annual CDOM accounted for by difference in hydraulic residence time. Similarly, Arts et al. [34] suggested that long residence time in prairie lakes (Canada) causes the DOC to become more UV transparent. Climate can affect both the watershed yield of DOC to lakes and coastal oceans and hydraulic residence time by influencing snowmelt, precipitation, evaporation, and watershed soil properties [13]. A period of warm and dry years resulted in a decline in DOC of Canadian shield lakes [104]. Temporal variation in DOC and CDOM absorption in lakes of N. Michigan (USA) was correlated with ice-out date and spring-summer precipitation [119].

At regional and larger scales several end members and other patterns of UV attenuation have emerged. The clearest lakes and ocean regions are those most isolated from terrestrial sources of CDOM and nutrients. A barren watershed containing little or no vegetation surrounds Crater Lake and Lake Vanda, and the permanently unmixed bottom waters likely serve as a trap for nutrients present in sinking biomass. The open ocean may appear to be equally isolated, but the connection with a deep-circulating source of CDOM and nutrients may

provide a low baseline level of UV attenuating substances that increases in the presence of deep mixing or upwelling. High elevation lakes tend to have lower levels of DOC [20] along with less vegetation in the watershed [62]. Mountain lakes of the Alps and Pyrenees [62] show an expected decrease in watershed vegetation with elevation, but when meadows and forest are compared at the same elevation the meadow-dominated watersheds have higher DOC levels. Lakes in contact with wetlands tend to have high levels of DOC (reviewed in [24]),but even higher levels occur in arid closed basin lakes [34].

Variations in DOC quality (DOC – specific attenuation and absorption) warrant further discussion. These variations can be divided into two related categories: changes in specific attenuation correlated with DOC concentrations, and changes in specific attenuation correlated with lake and watershed characteristics. The immediate basis for the power relationships between K_{d320} and [DOC] (Table 3) comes directly from the power relationship between a_{d320} and [DOC] (Table 2) for the data of Morris et al. [60]. But why should DOC quality change together with DOC concentration over the scale of lakes in this study? What determines the exponent in the power model relating specific absorption and DOC concentration?

Land cover in lake watersheds, climate, and hydraulic residence time influence the spatial pattern of DOC quality. Data from Laurion et al. [62] show that lakes with high-elevation watersheds had lower DOC concentrations than those at lower elevations in the same region. Lakes at similar elevations had lower DOC-specific attenuation if the watershed was rocky compared to watersheds with meadow or forested land cover. These data also showed that, for lake watersheds with similar land cover, DOC-specific attenuation was elevated when catchment area was more than 50 times larger than lake area, a characteristic associated with short residence times. For all the lake surveys in Table 2 and the majority in Table 3 the power equation exponent is greater than 1. These cover mountain lakes and wet areas at mid to high latitudes. The exceptions, where DOC-specific absorption varies inversely with DOC concentration, include ponds and lakes in the arid prairies of central Canada.

Temporal variation in DOC quality provides clues to explain the spatial variation. The decline of DOC-specific absorption in stratified surface waters [22, 23] and lake versus feeder stream [90] are attributed to cumulative photobleaching of the DOC pool. While photobleached DOC is in some cases subject to enhanced microbial utilization [105], the old and previously bleached DOC of saline prairie lakes is metabolized very slowly [90]. It is self-evident that photobleached DOC will not be dominant in the DOC pool while the rate of influx of non-bleached DOC is high. If hydraulic residence time is short then even low rates of DOC influx or production will be adequate to prevent accumulation of photobleached DOC.

3.4.1 A conceptual model for UV-DOC relationships

In most comparative studies to date the concentration and optical qualities of

DOC are the best predictors of UV attenuation. A conceptual model is proposed here to predict spatial and temporal patterns of UVR attenuation, including the relationship of K_{dUV} to [DOC], and α_{cdom} to [DOC], for all non-turbid aquatic systems. The DOC concentration will tend to be high in aquatic systems where influx or production is high relative to the rate of dilution or flushing by direct precipitation, snowmelt, or other source of low-DOC water. The [DOC] will also be high when a system with long hydraulic residence time experiences evaporation rates that exceed the rates of DOC degradation (microbial and photochemical). DOC concentration will be low in aquatic systems where DOC influx or production is low relative to rates of degradation or flushing with low-DOC water. DOC optical quality reflects the biotic source and the extent of photobleaching. For systems with short hydraulic residence times the DOC-specific absorption will be higher for sources from higher plant and lower for sources from the microbial community. Systems with long hydraulic residence times will tend to have low DOC-specific absorption when the long term rate of influx or production of DOC is slow compared to the rate of photobleaching by sunlight. DOC-specific absorption will become low as well in water that is seasonally isolated by density differences in a thin surface layer exposed to prolonged sunlight. Combining the processes influencing DOC concentration and specific absorption results in two hypotheses explaining the power relationships between K_d and [DOC] in equation (15). When DOC is not concentrated by water loss, the power exponent tends to exceed 1.0 because the systems with low [DOC] have experienced more cumulative photobleaching. In arid or frozen regions where cumulative water loss occurs in systems with long hydraulic residence time, the power exponent tends to be less than 1.0 because systems with high [DOC] have experienced more cumulative photobleaching.

3.5 Future directions

Fundamental to progress in understanding UV attenuation by natural waters is an improved understanding of absorption by pure water. Crater Lake and others like it offer the possibility to achieve optical closure for IOPs and AOPs with appropriate instrumentation. Advanced spectral absorption metres (e.g., the ICAM, [101,107]) should be extended into UV-B wavelengths and applied to testing ultra-pure water in the laboratory as well as the absorption of phytoplankton and other suspended particles at low concentrations. Temperature and salinity effects should be established for absorption by water in UV wavelengths.

Optical methods can be improved in large part by extending existing methods developed for visible wavelengths. A multispectral scalar UV sensor combined with existing uplooking and downlooking cosine sensors would improve our ability to measure $\bar{\mu}$ and thus to relate IOP's with AOP's. Lacking this, published algorithms for estimating $\bar{\mu}$ from multispectral reflectance meters should be extended into the UV wavelengths. Future underwater measurements should be more consistently combined with determination of sun angle (requires geographic coordinates and time of day) and the diffuse fraction for solar UV

irradiance in order that attenuation calculations can be standardized for sun and sky effects. CDOM measurements should be combined more often with measurement of [DOC] and with CDOM spectral fluorescence using the new method of McKnight et al. [80] to help characterize DOM optical qualities. At very low levels of CDOM the use of a proxy such as fluorescence will be needed for field measurements; even better would be an instrument like the Wetlabs AC-9 that operates in UV wavebands. CDOM calculations should consistently include corrections for scattering (where needed) and baseline offset, and regression techniques should avoid the noise region of the measuring instrument (where negative absorption coefficients can create a bias in calculated spectral slope). Spectral slope should be calculated for UV-B and UV-A wavebands. CDOM values should be checked against matched diffuse attenuation measurements to detect (and correct) errors where $K_d \leq (\alpha_{cdom} + \alpha_{phyto} + \alpha_{water})$. Measurement of UV absorption and attenuation by particles should be improved, including better methods for calibration of QFT using field samples. Phytoplankton pigment should be measured in combination with field optical measurements to develop trends in chlorophyll-specific absorption in the water column.

More field measurements of UV absorption by phytoplankton are needed and these should be scaled to chlorophyll concentration and evaluated for spatial and temporal patterns across gradients (trophic, UV, nutrient, grazing). The effect of depth and mixing should be evaluated for effects on UV exposure and on the response of cells to adjust UV-absorbing and photosynthetic pigments.

Sources and sinks of CDOM should be evaluated in lakes and ocean regions to achieve closure for carbon and optical budgets. Spatial correlation between microbial communities and CDOM is now possible with field absorption instruments but more work is also needed on microbial processing of DOC, especially in low-DOC systems. Effects of climate change on DOC and UV attenuation should be explored for different geographic regions, and should take into account changes in DOC-specific absorption as well as DOC concentration. Patterns of DOC-specific CDOM absorption and other DOC characteristics should be determined for a larger range of saline environments, including saline lakes, coastal and the open ocean, with comparisons between surface and deep water. More work is needed on the roles for watersheds and hydrology (including concentration of [DOC] by regulating its influx rate or by evaporative loss of water) in determining DOC optical qualities. The counterpart for oceans is to better determine basin-scale changes in CDOM quality as a function of water column biotic processes, photochemical processes, mixing, and other sources and sinks [74].

Acknowledgements

Support to the author for some of the published and unpublished data presented here has been provided by the Keck Foundation, the National Science Foundation, Lacawac Sanctuary, and Blooming Grove Hunting and Fishing Club. This manuscript was completed while the author was on sabbatical leave from Lehigh

University and supported in the laboratory of Horacio Zagarese, Univ. Comahue, Bariloche Argentina, by IAI, (Inter-American Institute for Global Change Research). Some unpublished data and instrument use at Crater Lake, OR have been provided by J.H. Morrow (Biospherical Instruments), Gary Larson (US Geologic Survey, Corvallis, OR) and Scott Girdner (National Park Service, Crater Lake). Helpful comments and unpublished data were also provided by Emmanuel Boss (Oregon State University). Other helpful comments were provided by an anonymous reviewer.

References

1. C.E. Williamson (1995). What role does UV-B radiation play in freshwater ecosystems? *Limnol. Oceanogr.*, **40**, 386–392.
2. C.E. Williamson, P.J. Neale, G. Grad, H.J. De Lange, B.R. Hargreaves (2001). Beneficial and detrimental effects of UV radiation on aquatic organisms: implications of variation in spectral composition *Ecol. Appl.* **11**, 1843–1857.
3. W. Preisendorfer (1976). *Hydrologic Optics* (vol. 1–6). U.S. Dept. of Commerce, NOAA, Honolulu, Hawaii.
4. G. Jerlov (1968). *Optical Oceanography*. Elsevier Publishing Co., Amsterdam.
5. C.D. Mobley (1994). *Light and Water: Radiative Transfer in Natural Waters*. Academic Press, San Diego.
6. J.T.O. Kirk (1994). *Light and Photosynthesis in Aquatic Ecosystems*, (2nd ed.). Cambridge University Press, Cambridge, 509 pp.
7. R.C. Smith, J.E. Tyler (1976). Transmission of solar radiation into natural waters. In: K.C. Smith (Ed.), *Photochemical and photobiological reviews*, (Volume 1, pp. 117–155). Plenum, New York.
8. R.C. Smith, K.S. Baker (1979). Penetration of UV-B and biologically effective doesrates in natural waters. *Photochem. Photobiol.*, **29**, 311–323.
9. K. S. Baker, R.C. Smith (1982). Spectral Irradiance penetration in natural waters. In: J. Calkins (Ed.), *The Role of Solar Ultraviolet Radiation in Marine Ecosystems, NATO Conference Series IV, Marine Sciences* (Vol. 7, pp. 233–246). Plenum Press, New York.
10. J.T.O. Kirk (1994). Optics of UV-B radiation in natural waters. *Arch. Hydrobiol. Beih., Ergbn. Limnol.*, **43**, pp. 226.
11. C.R. Booth, J.H. Morrow (1997). The Penetration of UV into Natural Waters, *Photochem. Photobiol.*, **65**, 254–257.
12. R.F. Whitehead, S.F. de Mora, S. Demers (2000). Enhanced UV radiation – a new problem for the marine environment. In: S. de Mora, S. Demers, M. Vernet (Eds), *The effects of UV Radiation in the Marine Environment*, (pp. 1–34). Cambridge University Press, Cambridge UK.
13. M.A. Xenopoulos, D.W. Schindler (2001). Physical factors determining ultraviolet radiation flux into ecosystems. In: C.S. Cockell and A.R. Blaustein (Eds), *Ecosystems, Evolution, and Ultraviolet Radiation*, (pp. 36–62). Springer, New York.
14. R.C. Smith, K.S. Baker (1986). Analysis of ocean optical data II. *Proc. SPIE, Ocean Optics VIII*, **636**, 95–107.
15. R.G. Zepp, D.M. Cline (1977). Rates of direct photolysis in the aquatic environment. *Environ. Sci. Technol.*, **11**, 359–366.
16. J.R. Zaneveld, E. Boss, A. Barnard (2001). Influence of surface waves on measured and

modeled irradiance profiles *Appl. Opt.*, **40**, 1442–1449.
17. H.R. Gordon (1989). Can the Beer-Lambert law be applied to the diffuse attenuation coefficient of ocean water? *Limnol. Oceanogr.*, **34**, 1389–1409.
18. R.C. Smith, K.S. Baker (1981). Optical Properties of the clearest natural waters (200–800 nm). *Appl. Opt.*, **20**, 177–184.
19. V.S. Kuwahara (2000). Variability in the relative penetration of ultraviolet radiation to photosynthetically available radiation in temperate coastal waters, Japan. *J. Oceanogr.*, **56**, 399–408.
20. C.E. Williamson, R.S. Stemberger, D.P. Morris, T.M. Frost, S.G. Paulsen (1996). Ultraviolet radiation in North American lakes: Attenuation estimates from DOC measurements and implications for plankton communities. *Limnol. Oceanogr.*, **41**, 1024–1034.
21. C.E. Williamson (1996). Effects of UV radiation on freshwater ecosystems. *Int. J. Environ. Stud.*, **51**, 245–256.
22. D.P. Morris, B.R. Hargreaves (1997). The role of photochemical degradation of dissolved organic carbon in regulating the UV transparency of three lakes on the Pocono Plateau. *Limnol. Oceanogr.*, **42**, 239–249.
23. A. Vodacek, N.V. Blough, M.D DeGrandpre, E.T. Peltzer, R.K. Nelson (1997). Seasonal variation of CDOM and DOC in the Middle Atlantic Bight: Terrestrial inputs and photooxidation, *Limnol. Oceanogr.*, **42**, 674–686.
24. P.A. Bukaveckas, M. Robbins-Forbes (2000). Role of dissolved organic carbon in the attenuation of photosynthetically active and ultraviolet radiation in Adirondack lakes. *Freshwat. Biol.*, **43**, 339–354.
25. R.W. Preisendorfer (1961). Application of radiative transfer theory to light measurements in the sea. *Union geod. Geophys. Inst. Monogr.*, **10**, 11–30, cited in [3].
26. K.S. Baker, R.C. Smith (1979). Quasi-inherent characteristics of the diffuse attenuation coefficient for irradiance, *Ocean Optics VI, SPIE*, **208**, 60–63.
27. V.N. Pelevin, V.A. Rutkovskaya (1977). On the optical classification of ocean waters from the spectral attenuation of solar radiation. *Oceanology*, **17**, 28–32.
28. R.C. Smith, K.S. Baker (1978). The bio-optical state of ocean waters and remote sensing. *Limnol. Oceanogr.*, **23**, 247–259.
29. H.R. Gordon (1976). Radiative transfer in the ocean: a method for determination of absorption and scattering properties. *Appl. Opt.*, **15**, 2611–2613.
30. M. Stramska, D. Stramski, B.G. Mitchell, C.D. Mobley (2000). Estimation of the absorption and backscattering coefficients from in-water radiometric measurements. *Limnol. Oceanogr.*, **45**, 628–641.
31. R.H. Stavn (1988). Lambert-Beer law in ocean waters: Optical properties of water and of dissolved/suspended material, optical energy budgets. *Appl. Opt.*, **27**, 222–231.
32. A.A. Gershun (1936). Fundamental ideas of the theory of a light field (vector methods of photometric calculations). (in Russian). *Izvestiya Akad. Nauk SSSR*, pp. 417–430, cited in Mobley [13].
33. N.M. Scully, D.R.S. Lean (1994). The attenuation of ultraviolet radiation in temperate lakes. *Arch. Hydrobiol. Ergebn. Limnol.*, **43**, 135–144.
34. M.T. Arts, R.D. Robarts, F. Kasai, M.J. Waiser, V.P. Tumber, A.J. Plante, H. Rai, H.J. de Lange (2000). The attenuation of ultraviolet radiation in high dissolved organic carbon waters of wetlands and lakes on the northern Great Plains. *Limnol. Oceanogr.*, **45**, 292–299.
35. K.W. Patterson, R.C. Smith, C.R. Booth (1997). A method for removing a majority of the error in PUV attenuation coefficients due to spectral drift in response with depth in the water column. *Ocean Optics XIII, SPIE*, **2963**, 737–742.

36. J.T.O. Kirk, B.R. Hargreaves, D.P. Morris, R.B. Coffin, B. David, D. Frederickson, D. Karentz, D.R.S. Lean, M.P. Lesser, S. Madronich, J.H. Morrow, N.B. Nelson, N.M. Scully (1994). Measurements of UV-B radiation in two freshwater lakes: an instrument intercomparison. *Arch. Hydrobiol. Beih Ergebn. Limnol.*, **43**, 71–99.
37. A. Morel, L. Prieur (1977). Analysis of variations in ocean colour. *Limnol. Oceanogr.*, **22**, 709–722.
38. J.T.O. Kirk (1980). Spectral absorption properties of natural waters: contribution of the soluble and particulate fractions to light absorption in some inland waters of southeastern Australia. *Aust. J. Mar. Freshwater Res.*, **31**, 287–296.
39. L. Prieur, S. Sathyendranath (1981). An optical classification of coastal and oceanic waters based on the specific spectral absorption curves of phytoplankton pigments, dissolved organic matter, and other particulate materials. *Limnol. Oceanogr.*, **26**, 671–689.
40. J.H. Sharp, R. Benner, L. Bennett, C.A. Carson, R. Dow, S.E. Fitzwater (1993). Re-evaluation of high temperature combustion and chemical oxidation measurements of dissolved organic carbon in seawater. *Limnol. Oceanogr.*, **38**, 1174–1782.
41. E. Aas, N.K. Højerslev (2001). Attenuation of ultraviolet irradiance in North European coastal waters. *Oceanologia*, **43**, 139–168.
42. R.C. Smith and K.S. Baker (1978). Optical classification of natural waters. *Limnol. Oceanogr.*, **23**, 260–267.
43. K.S. Baker, R.C. Smith (1982). Bio-optical classification and model of natural waters. 2 *Limnol. Oceanogr.*, **27**, 500–509.
44. E. W. Helbling, V. Villafane, O. Holm-Hansen (1994). Effects of ultraviolet radiation on Antarctic marine phytoplankton photosynthesis with particular attention to the influence of mixing. In: C.S. Weiler, P. A. Penhale (Eds). *Ultraviolet Radiation In Antarctica: Measurements and Biological Effects, Antarctic Research Series.* American Geophysical Union, Washington, D.C. (Vol. 62, pp. 207–227).
45. D. Karentz, S. McEuen, M.C. Land, W.C. Dunlap (1991). Survey of mycosporine-like amino acid compounds in Antarctic marine organisms: Potential protection from ultraviolet exposure. *Mar. Biol.*, **108**, 157–166.
46. L. Ayoub, B.R. Hargreaves, D.P. Morris (1997). UVR attenuation in lakes: Relative contribution of dissolved and particulate material. *Ocean Optics XIII, SPIE*, **2963**, 338–352.
47. H.M. Sosik (1999). Storage of marine particulate samples for light-absorption measurements. *Limnol. Oceanogr.*, **44**, 1139–1141.
48. C. Belzile, S.C. Johannessen, M. Gosselin, S. Demers, W.L. Miller (2000). Ultraviolet attenuation by dissolved and particulate constituents of first-year ice during late spring in an Arctic polynya. *Limnol. Oceanogr.*, **45**, 1265–1273.
49. C. Belzile, W.F. Vincent, M. Kumagai (2002). Contribution of absorption and scattering to the attenuation of UV and photosynthetically available radiation in Lake Biwa, *Limnol. Oceanogr.*, **47**, 95–107.
50. S.W. Jeffrey, H.S. MacTavish, W.C. Dunlap, M. Vesk, K. Groenewoud (1999). Occurrence of UVA- and UVB-absorbing compounds in 152 species (206 strains) of marine microalgae. *Mar. Ecol. Progr. Ser.*, **189**, 35–51.
51. S.E. Lohrenz (2000). A novel theoretical approach to correct for pathlength amplification and variable sampling loading in measurements of particulate spectral absorption by the quantitative filter technique. *J. Plankton. Res.*, **22**, 639–657.
52. A. Morel (1980). In-water and remote measurement of ocean colour. *Boundary-layer Meteorol.*, **18**, 177–201.
53. C.S. Yentsch (1962). Measurement of visible light absorption by particulate matter in

the ocean. *Limnol. Oceanogr.*, **7**, 207–217.
54. M. Kishino, N. Takahashi, N. Okami, S. Ichimura (1985). Estimation of spectral absorption coefficients of phytoplankton in the sea. *Bull. Mar. Sci.*, **37**, 634–642.
55. B.G. Mitchell D.A. Kiefer (1984). Determination of absorption and fluorescence excitation spectra for phytoplankton. In: O. Holm-Hansen, L. Bolis, R. Gilles (Eds). *Marine Phytoplankton and Productivity* (pp. 157–169). Springer-Verlag, Berlin.
56. B.G. Mitchell (1990). Algorithms for determining the absorption coefficient of aquatic particulates using the quantitative filter technique (QFT). *Ocean Optics X, SPIE*, **1302**, 137–148.
57. P.S. Kuhn, H.I. Browman, B. MacArthur, J.-F. St.-Pierre (1999). Penetration of ultraviolet radiation in the waters of the estuary and Gulf of St. Lawrence. *Limnol. Oceanogr.* **44**, 710–716.
58. A. Morel (1997). Optical properties of oceanic Case 1 waters, revisited. *Ocean Sciences XIII, SPIE*, **2963**, 108–114.
59. C.S. Yentsch, D.A. Phinney (1989). A bridge between ocean optics and microbial ecology. *Limnol. Oceanogr.*, **34**, 1694–1705.
60. D.P. Morris, H. Zagarese, C.E. Williamson, E.G. Balseiro, B.R. Hargreaves, B. Modenutti, R. Moeller, C. Queimalinos (1995). The attenuation of solar UV radiation in lakes and the role of dissolved organic carbon. *Limnol. Oceanogr.*, **40**, 1381–1391.
61. I. Laurion, W.F. Vincent, D.R.S. Lean (1997). Underwater Ultraviolet radiation: development of spectral models for northern high latitude lakes. *Photochem. Photobiol.*, **65**, 107–114.
62. I. Laurion, M. Ventura, J. Catalan, R. Psenner, R. Sommaruga (2000). Attenuation of ultraviolet radiation in mountain lakes: Factors controlling the among- and within-lake variability. *Limnol. Oceanogr.*, **45**, 1274–1288.
63. R. Sommaruga, R. Psenner (1997). Ultraviolet radiation in a high-mountain lake of the Austrian Alps: Air and underwater measurements. *Photochem. Photobiol.*, **65**, 957–963.
64. J. Shapiro (1957). Chemical and biological studies on the yellow organic acids of lake water, *Limnol. Oceanogr.*, **2**, 161–179.
65. N.K. Højerslev (1982). Yellow substance in the sea. In: J. Calkins (Ed.). *The Role of solar ultraviolet radiation in marine ecosystems* (pp. 263–279). Plenum Press, New York.
66. J.T.O. Kirk (1976). Yellow substance (gelbstoff) and its contribution to the attenuation of photosynthetically active radiation in some inland and coastal southeastern Australian waters. *Aust. J. Mar. Freshwater Res.*, **27**, 61–71.
67. A. Bricaud, A. Morel, L. Prieur (1981). Absorption by dissolved organic matter in the sea (yellow substance) in the UV and visible domains. *Limnol. Oceanogr.*, **26**, 43–53.
68. W.F. Vincent, R. Rae, I. Laurion, L. Howard-Williams, J. Priscu (1998). Transparency of Antarctic ice-covered lakes to solar UV radiation. *Limnol. Oceanogr.*, **43**, 618–624.
69. K.L. Carder, R.G. Stewart, G.R. Harvey, P.B. Ortner (1989). Marine humic and fulvic acids: effect on ocean color and fluorometric detection. *Limnol. Oceanogr.*, **34**, 68–81.
70. D.M. McKnight, R. Harnish, R.L. Wershaw, J.S. Baron, S. Schiff (1997). Chemical characteristics of particulate, colloidal, and dissolved organic material in Loch Vale watershed, Rocky Mountain National Park. *Biogeochemistry*, **36**, 99–124.
71. W.S. Pegau, J.R.V. Zaneveld (1993). Temperature-dependent absorption of water in the red and near-infrared portions of the spectrum. *Limnol. Oceanogr.*, **38**, 188–192.
72. W.S. Pegau, D. Gray, J.R.V. Zaneveld (1997). Absorption and attenuation of visible and near-infrared light in water: dependence on temperature and salinity. *Appl. Opt.*, **36**, 6035–6046.

73. R.J. Davies-Colley, W.N. Vant (1987). Absorption of light by yellow substance in freshwater lakes. *Limnol. Oceanogr.*, **32**, 416–425.
74. N.V. Blough, R. Del Vecchio (2002). Chromophoric dissolved organic matter (CDOM) in the coastal environment. In: D.A. Hansell and C.A. Carlson (Eds). *Biogeochemistry of Marine Dissolved Organic Matter* (pp. 509–546), Academic Press.
75. B.R. Hargreaves, C.L. Osburn, D.P. Morris, R.E. Moeller (2001). Spectral slope response to solar and biotic processes: Comparison of model with estimates from CDOM absorption and UV attenuation measurements. *Aquatic Sciences Meeting of ASLO*, Albuquerque, New Mexico, USA, February (abstract).
76. S. Markager, W.F. Vincent (2000). Spectral light attenuation and the absorption of UV and blue light in natural waters. *Limnol. Oceanogr.*, **45**, 642–650.
77. C.A. Stedmon, S. Markager, H. Kaas (2000). Optical properties and signatures of chormophoric dissolved organic matter (CDOM) in Danish coastal waters. *Estuarine, Coastal Shelf Sci.*, **51**, 267–278.
78. R.G. Wetzel (1992). Gradient-dominated ecosystems: sources and regulatory functions of dissolved organic matter in freshwater ecosystems. *Hydrobiologia*, **29**, 181–198.
79. C.E. Williamson, D.P. Morris, M.L. Pace, O.G. Olson (1999). Dissolved organic carbon and nutrients as regulators of lake ecosystems: Resurrection of a more integrated paradigm. *Limnol. Oceanogr.*, **44**, 795–803.
80. D.M McKnight, E.W. Boyer, P.K. Westerhoff, P.T. Doran, T. Kulbe, D.T. Anderson (2001). Spectrofluorometric characterization of dissolved organic matter for indication of precursor organic material and aromaticity. *Limnol. Oceanogr.*, **46**, 38–48.
81. H. DeHaan (1993). Solar UV-light penetration and photodegradation of humic substances in peaty lake water. *Limnol. Oceanogr.*, **38**, 1072–1076.
82. R.G. Zepp, P.F. Schlotzhauer (1981). Comparison of photochemical behavior of various humic substances in water: 3. Spectroscopic properties of humic substances. *Chemosphere*, **10**, 479–486.
83. A.J. Stewart, R.G. Wetzel (1981). Asymmetrical relationships between absorbance, fluorescence, and dissolved organic carbon. *Limnol. Oceanogr.*, **26**, 590–597.
84. S.A. Green, N.V. Blough (1994). Optical absorption and fluorescence properties of chromophoric dissolved organic matter in natural waters. *Limnol. Oceanogr.*, **39**, 1903–1916.
85. C.E. Del Castillo, F. Gilbes, P.G. Coble, F.E. Müller-Karger (2000). On the dispersal of riverine colored dissolved organic matter over the West Florida Shelf. *Limnol. Oceanogr.*, **45**, 1425–1432.
86. P.G. Coble (1996). Characterization of marine and terrestrial DOM in seawater using excitation-emission matrix spectroscopy. *Mar. Chem.*, **52**, 325–346.
87. W.F. Donahue, D.W. Schindler, S.J. Page, M.P. Stainton (1998). Acid-induced changes in DOC quality in an experimental whole-lake manipulation. *Environ. Sci. Technol.*, **32**, 2954–2960.
88. F.E. Hoge, A. Vodacek, N.V. Blough (1993). Inherent optical properties of the ocean: Retrieval of the absorption coefficient of chromophoric dissolved organic matter from fluorescence measurements. *Limnol. Oceanogr.*, **38**, 1394–1402.
89. S. Determann, R. Reuter, P. Wagner, R. Willkomm (1994). Fluorescent matter in the eastern Atlantic Ocean. Part 1: method of measurement and near-surface distribution. *Deep-Sea Res.*, **41**, 659–675.
90. M.J. Waiser, R.D. Robarts (2000). Changes in composition and reactivity of allochthonous DOM in a prairie saline lake. *Limnol. Oceanogr.*, **45**, 763–774.
91. N.B. Nelson, D.A. Siegel, A.F. Michaels (1998). Seasonal dynamics of colored dissol-

ved material in the Sargasso Sea, *Deep Sea Res, Part I*, **45**, 931–957.
92. C.S. Roesler (1998). Theoretical and experimental approaches to improve the accuracy of particulate absorption coefficients derived from the quantitative filter technique. *Limnol. Oceanogr.*, **43**, 1649–1660.
93. S. Tassan, G.M. Ferrari, A. Bricaud, M. Babin (2000). Variability of the amplification factor of light absorption by filter-retained aquatic particles in the coastal environment. *J. Plankton. Res.*, **22**, 659–668.
94. E. Urbach, K.L. Vergin, L. Young, A. Morse, G.L. Larson, S.J. Giovannoni (2001). Unusual bacterioplankton community structure in ultra-oligotrophic Crater Lake. *Limnol. Oceanogr.*, **46**, 557–572.
95. N.G. Jerlov (1950). Ultra-violet Radiation in the Sea. *Nature*, **166**, 111–112.
96. J.E. Tyler (1965). In situ spectroscopy in ocean and lake waters. *J. Opt. Soc. Am.*, **55**, 800–805.
97. R.C. Smith, J.E. Tyler (1967). Optical properties of clear natural water. *J. Opt. Soc. Am.*, **57**, 589–595.
98. J.E. Tyler, R.C. Smith (1966). Submersible spectroradiometer. *J. Opt. Soc. Am.*, **56**, 1390–1396.
99. R.C. Smith, J.E. Tyler, C.R. Goldman (1973). Optical properties and color of Lake Tahoe and Crater Lake. *Limnol. Oceanogr.*, **18**, 189–199.
100. R.C. Smith, B.B. Prezelin, K.S. Baker, R.R. Bidigare, N.P. Boucher, T. Coley, D. Karentz, S. MacIntyre, H.A. Matlick, D. Menzies, M. Ondrusek, Z. Wan, K.J. Waters (1992). Ozone depletion: ultraviolet radiation and phytoplankton biology in Antarctic waters. *Science*, **255**, 952–959.
101. R.M. Pope, E.S. Fry (1997). Absorption spectrum (380–700 nm) of pure water. II. Integrating cavity measurements. *Appl. Opt.*, **36**, 8710–8723.
102. J.B. Rasmussen, L. Godbout, M. Schallenberg (1989). The humic content of lake water and its relationship to watershed and lake morphometry. *Limnol. Oceanogr.*, **34**, 1336–1343.
103. S.A. Townsend, J.T. Luong-Van, K.T. Boland (1996). Retention time as a primary determinant of colour and light attenuation in two tropical Australian reservoirs. *Freshwat. Biol.*, **36**, 57–69.
104. D.W. Schindler, S.E. Bayley, B.R. Parker, K.G. Beaty, D.R. Cruikshank, E.J. Fee, E.U. Schindler, M.P. Stainton (1996). The effects of climatic warming on the properties of boreal lakes and streams at the Experimental Lakes Area, northwestern Ontario. *Limnol. Oceanogr.*, **41**, 1004–1017.
105. M.A. Moran, W.M. Sheldon, Jr., R.G. Zepp (2000). Carbon loss and optical property changes during long-term photochemical and biological degradation of estuarine dissolved organic matter. *Limnol. Oceanogr.*, **45**, 1254–1264.
106. R.E.H. Smith, J.A. Furgal, M.N. Charlton, B.M. Greenberg, V. Hiriart, C. Marwood (1999). Attenuation of ultraviolet radiation in a large lake with low dissolved organic matter concentrations. *Can. J. Fish. Aquat. Sci.*, **56**, 1351–1361.
107. R.M. Pope, A.D. Weidemann, E.S. Fry (2000). Integrating cavity absorption metre measurements of dissolved and suspended particles in ocean water. *Dynamics Atmos. Oceans*, **31**, 307–320.
108. V.S. Kuwahara, H. Ogawa, T. Toda, T. Kikuchi, S. Taguchi (2000). Variability of bio-optical factors influencing the seasonal attenuation of ultraviolet radiation in temperate coastal waters of Japan, *Photochem. Photobiol.*, **72**, 193–199.
109. W.L. Miller, M.A. Moran (1997). Interaction of photochemical and microbial processes in the degradation of refractory dissolved organic matter from a coastal marine environment. *Limnol. Oceanogr.*, **42**, 1317–1324.

110. J.E. Tyler, R.C. Smith, (1970). *Measurements of Spectral Irradiance Underwater*, Gordon & Breach, New York.
111. R.P. Dunne, B.E. Brown (1996). Penetration of solar UVB radiation in shallow tropical waters and its potential biological effects on coral reefs; results from the central Indian Ocean and Andaman Sea. *Mar. Ecol. Prog. Ser.*, **144**, 109–118.
112. F.M. Sogandares, E.S. Fry (1997). Absorption spectrum (340–640 nm) of pure water. I. Photothermal measurements. *Appl. Opt.*, **36**, 8699–8709.
113. T.I. Quickenden, J.A. Irvin (1980). The ultraviolet absorption spectrum of liquid water. *J. Chem. Phys.*, **72**, 4416–4428.
114. D.O. Hessen (1993). DNA-damage and pigmentation in alpine and arctic zooplankton as bioindicators of UV-radiation. *Verh. Internat. Verein. Limnol.*, **25**, 482–486 (cited in [10]).
115. I. Reche, M.L. Pace, J.J. Cole (1999). Relationship of trophic and chemical conditions to photobleaching of dissolved organic matter in lake ecosystems. *Biogeochemistry*, **44**, 259–280.
116. M.S. Twardowski, P.L. Donaghay (2001). Separating in situ and terrigenous sources of absorption by dissolved materials in coastal waters. *J. Geophys. Res.*, **106(C2)**, 2545–2560.
117. E. Aas, J. Høkedal, N.K. Højerslev, R. Sandvik, E. Sakshaug (2002). Spectral Properties of UV Attenuation in Arctic Marine Waters, pp. 23–56 in: *UV Radiation and Arctic Ecosystems, Ecological Studies* 153, Springer Verlag, Berlin 321 pp.
118. L.P. Boivin, W.F. Davidson, R.S. Storey, D. Sinclair, E.D. Earle (1986). Determination of the attenuation coefficients of visible and ultraviolet radiation in heavy water. *Appl. Opt.*, **25**, 877–882.